The Government of the Russian federation

Federal State Autonomous Educational Institution of Higher Professional Education

National Research University – Higher School of Economics

Faculty of Social Sciences, School of Psychology,
Master's program
"Cognitive sciences and technologies: from neuron to cognition"

Final qualifying work – MASTER THESIS

«Assessment of MEG-based functional connectivity during reward-based learning in anxiety»

Student group №МКОГН231
Saranskaia, Irina

Signature

Scientific adviser
Senior Research Fellow, PhD
Zinchenko, Oksana

Signature

Consultant
PhD
Herrojo Ruiz, M.

Signature

Moscow, 2025

Table of Contents

Chapter 1. Introduction

Anxiety is commonly experienced as a transient emotional response characterised by apprehension, tension, and worry about uncertain future events (Grupe and Nitschke, 2013). While adaptive in mobilising cognitive and physiological resources to cope with potential threats, anxiety becomes pathological when it is excessive, persistent and impairs daily functioning (Grupe and Nitschke, 2013; Bateson et al., 2011). In clinical contexts, anxiety disorders, such as generalised anxiety disorder, social anxiety disorder and panic disorder, are diagnosed according to standardised criteria and often require therapeutic intervention (American Psychiatric Association, 2022). By contrast, subclinical anxiety refers to elevated anxious feelings or behaviours that do not meet diagnostic thresholds but may nonetheless carry risk for future psychopathology (Gidron, 2013).

A key distinction in the study of anxiety is between state and trait anxiety. State anxiety denotes a fleeting, situation-dependent increase in self-reported tension or physiological arousal. In contrast, trait anxiety reflects a stable predisposition to perceive a wide range of stimuli as threatening and to respond with anxious affect across diverse contexts (Spielberger, 1983). Trait anxiety is not itself a medical diagnosis but rather a "personality dimension of neuroticism versus emotional stability" (Gidron, 2013). High trait-anxious individuals consistently overestimate threat, interpret ambiguous information negatively, and exhibit enhanced recall of threatening cognitive biases that contribute to vulnerability for affective disorders (Mathews and MacLeod, 2005).

Although trait anxiety does not equate to a clinical disorder, it has important implications for health and behaviour. It is routinely measured by the Trait version of the State–Trait Anxiety Inventory (STAI-T; Spielberger, 1983), and predicts outcomes in diverse medical settings, such as adaptation following myocardial infarction (Székely et al., 2007). Neuroimaging studies link high trait anxiety to hyperactivity of the amygdala and hypofunction of the dorsal anterior cingulate cortex during fear extinction, offering a mechanistic account of its role in stress reactivity (Sehlmeyer et al., 2011).

Contemporary theories of brain function cast perception and learning as forms of Bayesian inference under uncertainty. The predictive coding framework proposes that cortical hierarchies continuously generate top-down predictions and compare

them to bottom-up sensory inputs, propagating prediction errors to update internal models (Rao and Ballard, 1999; K. Friston and Kiebel, 2009). Predictive routing further specifies that these processes are mediated by distinct neural rhythms: fast γ-band oscillations conveying feedforward prediction errors and slower α/β rhythms carrying predictions via feedback pathways (Bastos et al., 2020). Hein et al. (2023) applied this framework to a volatile reward-learning paradigm, demonstrating that high-trait-anxious participants overestimate environmental volatility and exhibit exaggerated frontal γ responses alongside α/β suppression during the encoding of prediction errors (Hein et al., 2023).

Whereas oscillatory dynamics reveal local processing signatures, functional connectivity patterns characterise how distributed brain regions interact as coherent networks (Bassett and Gazzaniga, 2011; Buzsáki, 2006). Connectivity analysis can uncover alterations in large-scale circuits that underlie cognitive and affective biases in anxiety. Given the oscillatory disruptions observed by Hein et al. (2023), examining directed frequency-specific coupling may elucidate how trait anxiety disrupts the predictive routing across cortical hierarchies.

The present study aims to investigate magnetoencephalography (MEG) frequency-resolved functional connectivity differences between high- and low-trait-anxiety participants during a volatile reward-learning task previously examined by Hein et al. (2023). It is anticipated that high-trait-anxious individuals will show increased γ-band coupling and reduced α/β-band connectivity in fronto-cortical networks during prediction error encoding. The relevance of this research lies in integrating oscillatory and network-level perspectives on anxiety, thereby advancing our understanding of its computational and physiological substrates and informing potential biomarkers for intervention.

Chapter 2. Review of Key Concepts

2.1 Neural Changes Underlying Anxiety

Anxiety is a mental state characterised by prolonged apprehension and worry about undetermined events that may potentially have negative outcomes (Hein et al., 2023; Xu et al., 2019). While anxiety is deemed to have evolutionary value, allowing people to prepare for the detection and management of upcoming threats (Bateson et al., 2011), it is frequently accompanied by unpleasant and unwanted emotions and experiences that, on the contrary, prevent individuals from normal daily functioning. These maladaptive changes arise from the imbalances in large-scale brain network interactions and altered functional connectivity patterns. It has been shown that anxiety is associated with several alterations in the synchronisation and activation across networks, such as the default mode network (DMN), the affective network (AN), and the executive control network (ECN).

The DMN comprises brain regions that deactivate during attention-demanding, goal-directed tasks but activate during rest with eyes closed or fixated on a neutral stimulus (Raichle, 2015). Its core subdivisions include the ventral medial prefrontal cortex (vmPFC), dorsal medial prefrontal cortex (dmPFC), posterior cingulate cortex (PCC) with adjacent precuneus, and lateral parietal cortices (approximately Brodmann area 39) (Raichle, 2015). Anxiety, along with other psychopathological and neurodevelopmental conditions, such as depression (Coutinho et al., 2016), schizophrenia (Garrity et al., 2007; Öngür et al., 2010), bipolar disorder (Öngür et al., 2010), attention-deficit/hyperactivity disorder (Liddle et al., 2011; Uddin et al., 2008), and autistic spectrum disorders (Lynch et al., 2013; Padmanabhan et al., 2017), disrupts the integrity and synchrony of the DMN. One of the instances is the dissociation within the network. Coutinho et al. (2016) reported in a functional magnetic resonance imaging (fMRI) study that different parts of the network exhibit different patterns of connectivity in anxiety: anterior DMN regions (orbitofrontal cortex (OFC), mPFC, anterior cingulate cortex (ACC), middle frontal gyrus (MFG)) show increased functional connectivity with increasing anxiety, whereas posterior DMN regions (PCC, precuneus, inferior parietal gyrus) exhibit decreased connectivity under anxiety. Similarly, an fMRI study by Zhao et al. (2007) demonstrated the deactivation of inferior parietal cortex and key DMN hubs, mPFC and PCC, in the anxiety group, highlighting their important role in anxiety psychopathology. An elec-

troencephalography (EEG) study by Imperatori et al. (2019) further illustrated that higher levels of trait anxiety correspond to decreased θ-connectivity within DMN, between right mPFC and right PCC, and reduced β-connectivity between the right mPFC and right ACC. This finding supports the desynchronisation of DMN under anxiety. Notably, this pattern of "anterior-posterior DMN dissociation" (Coutinho et al., 2016) is observed in clinically depressed and anxious subjects (X. Zhu et al., 2012).

Beyond the DMN alterations, anxiety impairs communication between the affective and the executive control networks, which contributes to various anxiety disorders such as the generalised anxiety disorder, social anxiety disorder, and panic disorder (Xu et al., 2019). The ECN, also known as the lateral frontoparietal network, is a large-scale brain network, consisting of functionally connected areas: primarily, the regions of the PFC such as dorsolateral PFC (dlPFC) and dmPFC (Seeley et al., 2007), as well as regions of the parietal cortex (lateral posterior parietal cortex and inferior parietal lobule) (Xu et al., 2019). Additional regions include the posterior inferior temporal lobe and dorsomedial thalamus (Uddin et al., 2019). This network is involved in the regulation of higher cognitive functions such as decision-making, planning, task-switching, and working memory (Menon, 2011; Uddin et al., 2019). In anxiety, Geiger et al. (2016) reported reduced resting-state connectivity within the left ECN (inferior parietal gyrus, MFG, mPFC, OFC) alongside increased OFC–amygdala coupling, suggesting compromised top-down regulation of fear. However, this finding is not universal, and some connectivity studies report an opposing result of decreased connectivity between the amygdala and PFC (Hahn et al., 2011; Prater et al., 2013).

The amygdala, a deep nuclear complex, mediates emotion processing, in particular, fear, and reward-based motivation (LeDoux, 2007). It is a part of the affective network (AN) (or limbic network) which also includes the OFC, regions of the temporal cortex, deeply folded insular cortex, pallidum, and hippocampus (Kim et al., 2015). Various functional connectivity studies highlight the amygdala-prefrontal circuitry, which is altered in anxiety, leading to biased threat-related responses (Bishop, 2007; Prater et al., 2013): hyperactivation of the amygdala coupled with PFC hypoactivation correlates with heightened anxiety (Bishop, 2007). Anxiety infers weaker functional connectivity between the amygdala and PFC: specifically, amygdala–dlPFC connectivity decreases during fear processing (Prater et al., 2013), and amygdala–mPFC

connectivity diminishes at rest (M. Wang et al., 2021). Other large-scale brain networks, including the cingulo-opercular and ventral attention networks, also exhibit patterns of dysfunction in anxiety and anxiety disorders (Sylvester et al., 2012).

2.2 Predictive Coding and Routing and Oscillatory Alterations under Uncertainty in Anxiety

Difficulty in dealing with uncertainty is one of the key features of anxiety (Carleton et al., 2012; Grupe and Nitschke, 2013; Gu et al., 2020). Uncertainty about forthcoming events and their potential outcomes, though inevitable, diminishes our capacity to prepare effectively for what lies ahead (Grupe and Nitschke, 2013). The human brain endeavours to exploit all available but inherently insufficient information, encompassing both present cues and past experiences, to generate anticipatory models of the future. As Daniel Dennett observed in *Kinds of Minds*, "a mind is fundamentally an anticipator, an expectation-generator" (Dennett, 1997, p. 57), a capacity that functions as a survival mechanism by "allowing us to increase the odds of desired outcomes while avoiding or bracing ourselves for future adversity" (Grupe and Nitschke, 2013, p. 488). In increasingly volatile environments, where the hidden probabilistic contingencies of events shift more rapidly, individuals prone to anxiety tend to misestimate uncertainty, inflate perceived volatility and thereby the precision, or trust, they attach to incoming evidence (Hein et al., 2023). Classic behavioural studies reveal that participants high in trait anxiety fail to adjust their learning rates by environmental volatility (learning either too rapidly or too slowly) and consequently secure fewer rewards and make less consistent choices than their low-anxiety counterparts (Browning et al., 2015; Pulcu and Browning, 2019).

2.2.1 Predictive coding framework. The brain's capacity to form predictions from environmental inputs (an ability often compromised in anxiety) serves to make neural processing more efficient (Bastos et al., 2020). Within the broader family of Bayesian models of brain functioning, which posit that the brain represents sensory data probabilistically and constructs internal models of the world that are iteratively updated as new evidence is acquired (Clark, 2013; Knill and Pouget, 2004), the theory of predictive coding (PC) conceptualises the cortex as a hierarchical generative model that continuously compares top-down predictions with bottom-up prediction errors (PEs) (Rao and Ballard, 1999). According to this framework, the cortex transmits

"moment-to-moment predictions...to inhibit processing of expected inputs" (Bastos et al., 2020), since expected inputs, by their predictability, convey no novel information; conversely, unexpected sensory inputs, which deviate from the prediction, generate PEs that are not inhibited, are propagated forward, undergo further processing, influence subsequent behaviour, and inform the updating of beliefs about the environment (Bastos et al., 2020). Moreover, this account holds that the brain continually constructs and refines its internal models to forecast forthcoming sensory signals, such that any discrepancy between expectation and reality (that is, PEs) triggers model updating to minimise future prediction errors. Extending this notion, Karl Friston's free-energy principle asserts that an organism ensures its survival by minimising free energy (that is, the measurable surprise or uncertainty it encounters), thereby aligning its internal predictions with external reality (K. Friston and Kiebel, 2009).

Importantly, in anxiety, the overestimation of uncertainty disrupts this fundamental drive: when the brain erroneously treats too many inputs as surprising, PEs accumulate and model updating becomes erratic, thereby perpetuating a cycle of maladaptive coping (Grupe and Nitschke, 2013; Hein et al., 2023). The free-energy principle subsumes PC within a unified theoretical framework (simply put, that the brain's ultimate objective is to minimise surprise) and offers a coherent account of why anxious individuals struggle to resolve uncertainty and regulate their affective states: anxiety-prone brains treat too many signals as surprising and, thus, are unable to update their internal model of the environment stably.

2.2.2 Predictive routing framework. Predictive routing (PR) extends PC by integrating the function of neural oscillations into the cortical predictive-processing architecture (Gabhart et al., 2025). Bastos et al. (2020) recorded laminar activity in macaque visual (V4), posterior parietal (lateral intraparietal and area 7A), frontal eye field and PFC during tasks manipulating stimulus predictability, revealing two dynamic modes of stimulus processing. In the bottom-up mode, when a new sensory input is to be processed on every trial, thus associated with unpredictable stimuli, the superficial layers exhibited heightened spiking and γ-band power in all areas, with the predominance of feedforward Granger causality connections from the hierarchically lower sensory areas to higher cognitive areas. On the contrary, in the top-down mode, when the same sensory input is to be presented in every trial, there is no

need to completely process the new bottom-up inputs. Thus, predictable stimuli elicited enhanced α/β-power in deep layers of the PFC, which projected feedback to superficial sensory circuits, suppressing γ-band responses and spiking.

This mechanism negates the need for specialised error units: predictions are conveyed via deep-layer α/β oscillations that functionally inhibit superficial cortical circuits processing the expected inputs; when predictions are fulfilled, inhibited pathways yield minimal γ activity and spiking, whereas unpredicted inputs, whose pathways remain uninhibited, generate robust superficial-layer spiking and γ responses that propagate forward as PEs (Bastos et al., 2020). Although laminar specificity is pivotal for mechanistic insight, it lies beyond the scope of the present MEG study. Importantly, PR was first evident in the visual hierarchy (Rao and Ballard, 1999), but emerging data suggest that genuine PEs may originate at higher cortical levels. Gabhart et al. (2025) argue that the PFC orchestrates predictions through rhythm-specific channels, rendering predictive processing as much a cognitive operation as a sensory one (Gabhart et al., 2025). In paradigms based on probabilistic learning, such as the reward paradigm employed here, fronto-cortical γ dynamics should therefore constitute a primary focus of investigation.

2.2.3 Oscillatory signatures of anxious learning. Hein et al. (2023) applied the Bayesian PC framework to a binary probabilistic reward-learning task under volatility by fitting a three-level Hierarchical Gaussian Filter (HGF) to participants' choices and concurrently recording MEG. They showed that high-trait-anxious (HTA) individuals overestimated environmental volatility, which led to faster, more stochastic belief updates and a lower overall win rate compared to low-trait-anxious (LTA) controls (Hein et al., 2023). HTA participants exhibited enhanced γ-band responses in the ACC, dmPFC, and lateral OFC (lOFC), together with suppression of α/β activity in ACC during the encoding of unsigned, precision-weighted PEs (pwPEs), thereby identifying rhythm-based signatures of disrupted PC in anxiety (Hein et al., 2023).

Hierarchical Gaussian Filter The HGF conceptualises learning as a hierarchy of coupled Gaussian random walks (Mathys et al., 2011; Mathys et al., 2014). Level 1 ($i = 1$) represents the binary sensory outcome (win/loss), level 2 ($i = 2$) encodes beliefs about the hidden reward probability and is the locus of belief updating, and

level 3 ($i = 3$) tracks the log-volatility of those probabilities, modulating the update rate: higher estimated volatility increases the variance of level-2 beliefs and, thus, the learning rate, whereas lower volatility stabilises those beliefs.

Belief updates follow (Mathys et al., 2011; Hein et al., 2023):

$$\Delta\mu_i^{(k)} = \tilde{\pi}_i^{(k)} delta_{i-1}^{(k)},$$

where $\Delta\mu_i^{(k)}$ is the change in the posterior mean of the level-i belief distribution on trial k,
$\delta_{i-1}^{(k)}$ is the prediction error from level $i-1$,
$\tilde{\pi}_i^{(k)} = \hat{\pi}_{i-1}^{(k)}/\pi_i^{(k)}$ is the precision ratio, which weighs the influence of precision.
Precision is defined as the inverse of variance:

$$\pi_i^{(k)} = \frac{1}{\sigma_i^{(k)}},$$

and emerges directly from the model's uncertainty dynamics (Mathys et al., 2011). Each level's variance, $\sigma_i^{(k)}$, is governed by its evolution parameters (the tonic step-size ω_i and the coupling strength κ_i, fixed to one in the Hein et al. (2023) study) and, for level 2, by the previous trial's level-3 posterior mean:

$$\sigma_2^{(k)} = \sigma_2^{(k-1)} + \exp^{\kappa\mu_3^{(k-1)}+\omega},$$

where $\mu_3^{(k-1)}$ is the previous trial posterior mean of log-volatility. Because $\pi_i^{(k)} = 1/\sigma_i^{(k)}$, higher estimated volatility (larger σ) yields lower precision and vice versa (Mathys et al., 2011).

Sensory precision at level 1 is determined by the Bernoulli outcome likelihood and is therefore constant:

$$q(x_1^{(k)}) = \text{Bernoulli}(x_1^{(k)}; \mu_1^{(k)}),$$

where $q(x_1^{(k)})$ is the inferred belief distribution over $x_1^{(k)}$,
$x_1^{(k)}$ is the hidden state, which at level 1 is the actual observed outcome, with $\mu_1^{(k)} = u^{(k)}$ and $\sigma_1^{(k)} = \mu_1^{(k)}(1-\mu_1^{(k)})$, where $u^{(k)}$ is the sensory input, observed win or loss at level 1.

Fitting the HGF yields subject-specific parameters that generate trial-by-trial

variances and hence precision estimates, which in turn weight each PE: high precision amplifies unexpected inputs, whereas low precision attenuates them, implementing a Bayes-optimal surprise-minimisation strategy analogous to the Kalman filter (Feldman and Friston, 2010; Knill and Pouget, 2004).

Applications of the HGF Since its introduction, the HGF has become a standard tool in computational neuroscience for modelling learning under uncertainty. Early studies used it to capture midbrain and basal–forebrain PE signals in sensory tasks (Iglesias et al., 2013; Iglesias et al., 2019) and to reveal stress-induced shifts in volatility estimates (de Berker et al., 2016). Subsequent research extended the HGF to clinical populations, demonstrating superior fits over simple reinforcement-learning models in anxiety (Hein et al., 2021) and bipolar disorder (Ivanova et al., 2025), and has employed it to dissect visual mismatch responses in EEG (Stefanics et al., 2018), probe hierarchical social inference (Diaconescu et al., 2014), and explain hallucinations in psychosis via aberrant precision-weighting (Powers et al., 2017). Although alternative Bayesian models, such as the joint estimation of volatility and stochasticity of Piray and Daw (2021), offer promising frameworks, differences in inversion methods currently preclude direct comparison (Hein et al., 2023). Nevertheless, the HGF's hierarchical structure, trial-by-trial precision estimation, and biological plausibility make it a versatile framework for linking computational mechanisms of uncertainty to neural dynamics.

Predictive coding and oscillatory dynamics Under the PC framework, fast γ oscillations convey bottom-up PEs, while lower α and β rhythms carry top-down predictions and precision estimates (Bastos et al., 2020). Overestimation of volatility in HTA individuals, thus, predicts an up-weighting of pwPEs and subsequent amplified feedforward γ activity with the suppression of α/β activity (Bastos et al., 2020). Hein et al. (2023) observed precisely these oscillatory signatures, providing a mechanistic account of circuit-level dysregulation in anxious learning.

2.3 Connectivity Analysis

Cognitive processes are supported by complex temporally and spatially distributed networks (Bassett and Gazzaniga, 2011; Bassett et al., 2018; E. Rolls et al., 1997; Smallwood et al., 2021). Understanding how these networks are formed and

broken apart, how they change, and how they communicate with other networks and within themselves is the key to deciphering psychological and pathological states of the brain. Networks are characterised by functional and structural connectivity, which can be derived using various neuroimaging techniques. The two have been researched in relation to one another, highlighting the following ideas:

- Functional connectivity is a reflection of structural composition (Greicius et al., 2009);
- Functional connectivity might be predicted from structural connections, assuming that strength, persistence, and spatial distribution are constrained by the large-scale anatomical structure of the human brain (Honey et al., 2009).

While structural connections are deemed to be more persistent on a shorter time scale (up to minutes), functional connectivity is highly time-dependent and could change in a matter of fractions of milliseconds (Sporns, 2013). Given the difficulty of characterising dynamic connections formed on the microscopic level (Seguin et al., 2023) and the inability to control for those changes, identifying reliable functional connectivity patterns becomes a challenging issue. Nonetheless, it is an important methodological approach to explore cognitive and perceptual processes such as attention (Madhyastha et al., 2015; Parks and Madden, 2013), decision-making (Cohen et al., 2005; Li et al., 2013), visual perception (Ardila et al., 2015; Deshpande et al., 2008), etc. Neurodegenerative disorders (slowly progressing disorders of the nervous system characterised by necrosis) such as the Alzheimer's disease, Parkinson's disease, and dementia (Dugger and Dickson, 2017), are also characterised by the structural and functional changes in the brain: for example, Alzheimer's disease is characterised by the damage to one of the large-scale brain networks – DMN (Hohenfeld et al., 2018). Other pathological conditions, such as major depressive disorder (Manoliu et al., 2014; Liu et al., 2018), schizophrenia (Palaniyappan et al., 2011; Palaniyappan and Liddle, 2012), post-traumatic stress disorder (Abdallah et al., 2019; Nicholson et al., 2020; Szeszko and Yehuda, 2019), obsessive-compulsive disorders (Peng et al., 2014; Reess et al., 2016) and many others are characterised by the dysfunction and/or disrupted connectivity within and between brain networks.

Connectivity analysis is, thus, aimed at "untangling" recorded signals into more or less coherent patterns of synchronised neuronal activity, revealing how distributed

brain regions couple and interact over time. The hypothesis that synchronisation of the neural oscillations enables dynamical coordination as it reflects the fluctuations of the rhythmic excitability among local neuronal populations, facilitating the flow of neural information within the network (Buzsáki, 2006; Fries, 2015; Singer, 1999) has gained broad acceptance within the field of neuroscience (Bastos and Schoffelen, 2016), making connectivity analysis extremely popular for characterising interactions within and between brain networks.

2.3.1 Types of connectivity. As stated above, connectivity is a comprehensive term combining anatomical connections and inferred dependencies between the activity of distinct regions. On a larger scale, these two types of connections are intrinsically organised in a way that provides the necessary means for near-optimal information processing (Lang et al., 2012). However, when performing brain connectivity analysis, it is important to differentiate between the two types of connectivity (Sporns, 2013). Structural connectivity describes anatomical links between different neural elements (be it individual neurons, neuronal ensembles, and large brain networks), and such data might be extracted using histological methods for tracing neuronal pathways (Meijering, 2010); electron microscopy which allows for ultra-high-resolution (Abbott et al., 2020); diffusion MRI for revealing white matter fibre tracts (Yeh et al., 2021) or structural T1- and T2-weighted MRI to infer large-scale brain network architecture (Ganzetti et al., 2015; Wittayer et al., 2023), and others, such as light-microscope tract tracing (Osten and Margrie, 2013) or tissue clearing and light-sheet microscopy (Ueda et al., 2020).

While structural connections are physical in nature, functional connectivity patterns may only be detected through data analysis. Functional connections do not necessarily reflect the presence of physical connections: they reflect the statistical relationships between different regions, whether they are structurally connected or not, local or distant (Lang et al., 2012); thus, it is not a physical entity, but rather a statistical concept. Neural time series can be extracted using neuroimaging techniques, including MEG, EEG, and fMRI. Statistical analysis relies on a variety of statistical measures, which will be described in more detail below. However, it is important to note here that those measures could be directed and non-directed, highlighting different aspects of connectivity. While non-directed metrics characterise statistical dependencies regardless of their direction and causal influence, directed measures

aim to describe the influence one region exerts upon another (K. J. Friston, 2011), reflecting specific relations between the signals. Such directed connections fall under the definition of "effective connectivity," which strives to explain observed functional dependencies.

While some explicitly differentiate between the two, functional and effective connectivity (K. J. Friston, 2011; Haufe et al., 2013; Lang et al., 2012; Sporns, 2013), others are not as strict (Bastos and Schoffelen, 2016; Pellegrini et al., 2023). In this paper, this distinction is addressed by differentiating between connectivity types using directed and non-directed measures, which correspond to effective and functional connectivity, respectively.

2.3.2 Measures of connectivity. It has been stated that connectivity measures are divided into non-directed and directed. Additionally, within directed and non-directed measures, another differentiation can be made based on the assumption of linearity: model-based measures assume that all interactions are linear, while model-free measures do not require this assumption (Bastos and Schoffelen, 2016). The third basis for differentiation involves the specific component of the signal that is of interest, whether it is phase-to-phase coupling, phase-to-amplitude coupling, or amplitude-to-amplitude coupling. Generally, oscillations, which could be represented in the time or frequency domain, can be characterised by three main components: phase, power (or amplitude, which is the square root of power), and frequency (Cohen, 2014). The phase of the signal refers to the timing of the oscillation, the amplitude measures the magnitude of the change of the oscillation, and the frequency refers to how fast the oscillation is. Phase-based connectivity measures are aimed at assessing phase-to-phase coupling and are widely used (Bastos and Schoffelen, 2016; Cohen, 2015) under the hypothesis that phase changes and synchrony of these changes underlie neuronal communication (Bastos et al., 2015).

While sensors record activity as a function of time, neural time series are conveniently represented and analysed in the frequency domain. Neural oscillations reflect the electrical activity of neuronal populations, and this rhythmic brain activity is composed of multiple frequencies simultaneously. These frequencies can be separated using various signal-decomposition techniques such as Fourier decomposition, wavelet transform, Hilbert transformation with band-pass filtering, etc. (Bastos and Schoffelen, 2016; Brookes et al., 2004; Cohen, 2014; Zhou et al., 2020). Rhythmic

oscillations are grouped into different bands by the frequency intervals that underlie different cognitive processes (Cannon et al., 2014; Thut et al., 2012; Ward, 2003). Subsequently, connectivity measures estimated in the frequency domain can be used to assess such neuronal interactions. Frequency-resolved connectivity measures are particularly well suited to the PR framework, which posits that γ-band oscillations convey PEs and are enhanced during processing of unexpected stimuli, whereas α/β activity mediates top-down inhibition of γ activity when inputs are predictable.

This chapter will focus on the model-based measures of phase relations. Linear methods are able to capture oscillatory interactions, given the assumption that phase coupling is the primary regulator of such interactions. (Bastos and Schoffelen, 2016; Pellegrini et al., 2023). Several measures will be described: coherence, coherency, additional metrics focused on the imaginary part of coherency (the imaginary part of coherency and maximised imaginary coherency), Granger causality with its time-reversed version, and phase-slope index.

A substantial amount of these measures is derived from the cross-spectrum, which is used to define the relationship between two time series in the frequency domain. Cross-spectrum can be defined as the Fourier transform of cross-covariance, which measures how common activity between two processes is distributed across frequencies. Cross-covariance function, in turn, measures one signal's covariance with another at each pair of time points. Equivalently, the cross-spectrum can also be computed as follows (Nunez et al., 1997):

$$S_{xy}(f) =< x(f)y^*(f) >,$$

where $S_{xy}(f)$ is the cross-spectrum defined at frequency f,
$x(f)$ is the Fourier transform of the multivariate time series $\overline{x}(t)$, where $t \in \{1, \ldots, T\}$ refers to indices of time samples,
$y^*(f)$ is the complex conjugate of the Fourier transform of the multivariate time series $\overline{y}(t)$ where $t \in \{1, \ldots, T\}$ refers to indices of time samples,
$< \cdot >$ operation denotes the expectation value (average).

2.3.3 Non-directed metrics. Non-directed measures do not assess the influence one time series has over another, they are merely an indication of statistical correlation between the two time series. One such measure to quantify phase synchrony is the coherence, which is the equivalent of the cross-correlation function in the time

domain. Coherence is a real-valued number which provides information about the strength of linear correlation between the two time series (Pellegrini et al., 2023) and ranges from 0 to 1, where 0 indicates no linear relationship at a specific frequency, while 1 indicates an ideal linear relationship at a specific frequency. Coherence is derived from coherency, a complex-valued measure that quantifies both the strength of correlation between the two time series and their average phase difference. As given by Nunez et al. (1997), coherency is defined as the normalised cross-spectrum:

$$C_{xy}(f) = \frac{S_{xy}(f)}{\sqrt{S_{xx}(f)S_{yy}(f)}},$$

where $C_{xy}(f)$ is the coherency defined at frequency f,
$S_{xy}(f)$ is the cross-spectrum defined at frequency f,
$S_{xx}(f)$ is the power spectral density (PSD) of the Fourier transform of the signal $\overline{x}(t)$,
$S_{yy}(f)$ is the PSD of the Fourier transform of the signal $\overline{y}(t)$.

The PSD used in the calculation represents the amount of power present in the signal at a specific frequency. Coherence is derived from the coherency by taking the absolute value: $\text{COH}_{xy}(f) = |C_{xy}(f)|$, where $\text{COH}_{xy}(f)$ is the coherence defined at frequency f, $C_{xy}(f)$ is the coherency defined at frequency f, and $|\cdot|$ operation refers to taking the absolute value defining the magnitude of the measure.

Coherence captures both zero-lag interactions and non-zero-lag synchronisation. Volume conduction of the head tissues introduces instantaneous (zero-lag) mixing of sensor signals, so that many spurious connections arise purely from spatial leakage rather than true neuronal coupling (Nolte et al., 2004). To identify genuine brain interactions, Nolte et al. (2004) proposed the imaginary part of coherency, which by definition is sensitive only to non-zero-lag synchronisation.

Expressing the coherency in polar coordinates, we obtain

$$|C_{xy}(f)|e^{i\Delta\varphi(f)},$$

where $\Delta\varphi(f)$ is the phase difference at frequency f. By expanding using Euler's formula, we obtain:

$$C_{xy}(f) = |C_{xy}(f)|\big[\cos\Delta\varphi(f) + i\sin\Delta\varphi(f)\big],$$

so that taking the imaginary part converts to

$$\Im\{C_{xy}(f)\} = |C_{xy}(f)| \sin\big(\Delta\varphi(f)\big).$$

Since $\sin(0) = 0$, any zero-lag component ($\Delta\varphi = 0$) contributes nothing to $\Im\{C_{xy}(f)\}$, and only interactions with a non-zero phase delay remain. Under the assumption that volume conduction is effectively instantaneous, taking the imaginary part, thus, discards spurious zero-lag synchrony while preserving true, time-lagged neuronal coupling. Formally, the imaginary coherency is defined as $\text{ImCOH}_{xy}(f) = \Im\big\{C_{xy}(f)\big\}$, whose absolute values range from 0 (no consistent non-zero-lag phase relationship) to 1 (perfectly consistent non-zero-lag synchronisation) (Bastos and Schoffelen, 2016).

The metrics described above are not meant to provide one aggregated functional connectivity score, but instead, they measure connectivity for all pairs of sensor channels or regions of interest (ROIs). A single functional connectivity measure can be obtained by averaging all $\text{COH}_{xy}(f)$ or $\text{ImCOH}_{xy}(f)$ functional scores (Pellegrini et al., 2023). Between $\text{COH}_{xy}(f)$ and $\text{ImCOH}_{xy}(f)$, the former is non-robust, while the latter is. $\text{ImCOH}_{xy}(f)$ is robust to volume conduction artefacts, meaning that it vanishes for independent sources that do not interact in any way, even if they are mixed and detected by multiple sensors. Thus, if the metric is non-zero, it is a signature of true interactions between brain sources (Ewald et al., 2012). Another such measure is the maximised imaginary coherency (MIC). It generalises $\text{ImCOH}_{xy}(f)$, which explains its robustness against spatial leakage. Apart from being robust, it also deviates from the previous coherency-based methods by being multivariate, while the former ones are bivariate, that is, estimating connectivity between a pair of signals. Multivariate measures, on the other hand, capture interactions between groups of signals. The multivariate approach offers methodological improvements to the connectivity analysis, such as reducing the biased estimations of the connectivity based on the spatial proximity of sensors (Ewald et al., 2012), easier results interpretation following the dimensionality reduction, and enhanced SNR.

Going beyond pairwise descriptions, multivariate functional connectivity metrics, such as canonical coherence (Vidaurre et al., 2019), regression cortico-muscular coherence (Bayraktaroglu et al., 2011), and the multivariate interaction measure (Ewald et al., 2012), simultaneously consider the joint dynamics of multiple time series to reveal higher-order interdependencies. By finding optimal linear combinations

of all signals in each set that maximise a coherence-based criterion, these methods inherently reduce dimensionality while focusing on the strongest network modes (Bayraktaroglu et al., 2011; Vidaurre et al., 2019). This multivariate framework mitigates spurious connections, improves statistical power by aggregating across redundant sources, and facilitates the construction of more complex structures that allow for exploring the network connectivity, such as hypergraphs in which hyperedges link multiple regions according to their joint connectivity strength (L. Zhu et al., 2023).

MIC utilises the projection operation. If we adopt the definitions from the previous measures, then $x(f)$ and $y(f)$ denote the Fourier transform of multivariate time series $\overline{x}(t)$ and $\overline{y}(t)$, respectively. Each of these defines a linear subspace of dimension K and L, where K and L refer to the number of data dimensions arising from the three dipole orientations along the x, y, and z axes. A neural dipole represents the current generated by a neuronal population with a given orientation (fixed or free, thus referring to the three dipole orientations) and location. MIC seeks linear projections from two multi-dimensional subspaces to two one-dimensional spaces via weight vectors a and b, such that the imaginary coherency between the projected signals is maximised Pellegrini et al., 2023. Formally, as shown by Ewald et al. (2012) and Pellegrini et al. (2023), MIC is defined as:

$$\mathrm{MIC}_{xy}(f) = \max_{a,b} \left(\frac{a^T \, \overline{S}^{\Im}_{xy}(f) \, b}{\|a\| \, \|b\|} \right),$$

where a and b are the projection weight vectors that correspond to subspaces of $x(f)$ and $y(f)$, respectively,
$\overline{S}^{\Im}_{xy}(f)$ is the whitened imaginary part of the cross-spectrum $S_{xy}(f)$.

The use of the imaginary part of the cross-spectrum ensures that only genuine interactions are captured, as it vanishes for non-interacting sources (Ewald et al., 2012).The whitening operation on $\Im\{S_{xy}(f)\}$ normalises the power across all frequencies by removing the auto-correlations (correlation of a signal with a time-delayed version of itself) within each time series, thereby mitigating the influence of the volume conduction artefacts (Ewald et al., 2012). Volume conduction induces spatial correlations when a single source is detected by multiple sensors, leading to spurious coherency; whitening counteracts this by equalising frequency power and enhancing the signal of true neuronal interactions. MIC is bounded between 0 and 1,

where 0 indicates an absence of functional connectivity and 1 denotes an optimally coherent interaction.

2.3.4 Directed metrics. Directed measures evaluate both the existence of an interaction and its direction of influence between time series (Haufe et al., 2013). Although the imaginary part of coherency, $\text{ImCOH}_{xy}(f)$, is formally undirected, its sign can hint at temporal ordering: a positive $\text{ImCOH}_{xy}(f)$ generally implies that $x(f)$ leads $y(f)$, whereas a negative value suggests that $x(f)$ lags $y(f)$ (Haufe et al., 2013). However, due to the periodicity of the oscillation, it cannot be unambiguously established which signal truly precedes the other. To resolve this, Nolte et al. (2008) proposed the phase-slope index (PSI), which pools phase information across a frequency band to emphasise consistent non-zero phase lags (Nolte et al., 2008). The PSI is founded on the principle that a genuine interaction incurs a frequency-dependent phase delay: when waves travel at comparable speeds, the phase difference between the source and the destination increases with frequency, leading to an anticipated positive slope in the phase spectrum (Nolte et al., 2008). Nolte et al. (2008) suggest the following equation to estimate PSI:

$$\Psi_{xy} = \Im\left(\sum_{f \in F} C_{xy}(f + \delta f) C^*_{xy}(f)\right)$$

where Ψ_{xy} is the PSI estimated for the Fourier transforms $x(f)$ and $y(f)$ of the signals $\overline{x}(t)$ and $\overline{y}(t)$, respectively,
$C_{xy}(f)$ is the complex coherency defined at frequency $f \in F$ set of defined frequencies over which the slope is summed,
$C^*_{xy}(f)$ is the complex conjugate of the coherency,
δf is the spectral resolution (the smallest frequency difference that can be distinguished).

PSI utilises the temporal argument to estimate the direction of the interaction: the preceding process is assumed to drive the lagging one. It is a signed metric ranging from negative to positive values, where the sign and the magnitude indicate the direction of the interaction and its strength. The causal direction is estimated to go from $x(f)$ to $y(f)$ if Ψ_{xy} is positive, and from $y(f)$ to $x(f)$ if Ψ_{xy} is negative. Values of $\Psi_{xy} \approx 0$ imply little to no consistent directional coupling. Because PSI is derived from the imaginary part of coherency and aggregates phase information across fre-

quencies, it remains robust to volume-conduction artefacts and non-interacting signal mixtures (Haufe et al., 2013; Nolte et al., 2008).

Granger causality The temporal argument behind the estimation of the direction of an interaction underlies the conceptual basis of another measure – Granger causality (GC). Although it was originally developed in the field of econometrics (Granger, 1969), it is now widely used to analyse a variety of time-series problems, including applications in neuroscience. GC evaluates directed dependencies by testing whether past values of one time series improve the "prediction" of another beyond its own history (Granger, 1969; Pellegrini et al., 2023). In the time domain, GC is based on fitting autoregressive (AR) models: for two univariate time series $\overline{x}(t)$ and $\overline{y}(t)$, one compares:

$$\overline{x}(t) = \sum_{n=1}^{p} A_n \overline{x}(t-n) + \epsilon_x(t),$$
$$\overline{x}(t) = \sum_{n=1}^{p} A_n \overline{x}(t-n) + \sum_{n=1}^{p} B_n\, \overline{y}(t-n) + \epsilon_{x|y}(t),$$

where p is the model order,

A_n and B_n are the AR coefficients,

ϵ_x and $\epsilon_{x|y}$ are the residual errors. The signal $\overline{x}(t)$ is said to be Granger-caused by $\overline{y}(t)$ if the past values of $\overline{y}(t)$ enhance the "prediction" of future values of $\overline{x}(t)$ beyond what can be estimated solely based on the past values of $\overline{x}(t)$ (Pellegrini et al., 2023). GC from $\overline{y}(t)$ to $\overline{x}(t)$ could be defined as "the natural logarithm of a ratio of residual variances from two different models" (Bastos and Schoffelen, 2016, p. 8):

$$F_{y\to x} = \ln \frac{\mathrm{Var}[\epsilon_x(t)]}{\mathrm{Var}[\epsilon_{x|y}(t)]}.$$

Since the logarithm of a ratio exceeds zero exactly when the numerator is larger, $F_{y\to x} > 0$ precisely when including past values of $\overline{y}(t)$ reduces the error variance of; in that case, $\overline{y}$ is said to Granger-cause $\overline{x}$. Estimation of the AR coefficients and residual variances is typically performed via ordinary least squares (Pierce, 1971), method of moments (Kelejian and Prucha, 1999) or maximum likelihood algorithm (W. Wang et al., 2011); the statistical significance of $F_{y\to x}$ can be assessed using F-tests based on the ratio of estimated residual covariances (Haufe et al., 2013). In the

frequency domain, a spectrally resolved extension of GC is used, which involves the calculation of the additional spectral transfer matrix, describing how one time series' frequency components are linearly transformed to produce the frequency components of another time series (Pellegrini et al., 2023).

Time-reversed Granger causality GC is not a robust measure of connectivity (Haufe et al., 2013), and it fails to account for the volume conduction artefacts, thus, mutually "improving" the prediction between two channels, since instantaneous mixtures can induce apparent predictability in both directions (Haufe et al., 2013). A robust measure, called time-reversed Granger causality (TRGC), mitigates this by computing GC on both the original and a time-reversed version of the data (Pellegrini et al., 2023). TRGC, like the previous measures, reflects the statistical dependency between time series. Denote the frequency-resolved net GC from $\overline{x}$ to $\overline{y}$ at frequency f as

$$\mathcal{F}^{\text{net}}_{x\to y}(f) = \mathcal{F}_{x\to y}(f) - \mathcal{F}_{y\to x}(f),$$

where $\mathcal{F}_{x\to y}(f)$ is the Granger score at f and $\mathcal{F}_{y\to x}(f)$ is its converse (Winkler et al., 2016).

To compute the time-reversed counterpart, each series is reversed in time, $\overline{x}(t) \to \overline{x}(-t)$ and likewise for $\overline{y}(t)$, and the multivariate AR is refitted using the transposed autocovariance sequence $G^{\text{TR}}_{[xy]}(p) = G^{\text{T}}_{[xy]}(p)$, $p \in \{0, 1, \ldots, N_p\}$ (Pellegrini et al., 2023). This yields the reversed-order net GC $\mathcal{F}^{\text{TR net}}_{x\to y}(f)$. Finally, the TRGC is defined as

$$\mathcal{F}^{\text{TRGC}}_{x\to y}(f) = \mathcal{F}^{\text{net}}_{x\to y}(f) - \mathcal{F}^{\text{TR net}}_{x\to y}(f),$$

so that genuine delayed interactions, which diminish under time reversal, are preserved, while zero-lag volume conduction artefacts cancel out (Haufe et al., 2013; Pellegrini et al., 2023). TRGC is implemented in the ROIconnect EEGLAB plugin, enabling straightforward computation of both GC and TRGC on source-reconstructed EEG and MEG data (Pellegrini et al., 2023).

2.3.5 Additional constraints to connectivity analysis.

The described methods assist in estimating functional connectivity; however, the analysis of this connectivity is limited by various issues and confounding factors. These constraints

introduce an uncertainty in the estimation of functional connectivity, posing two main questions: whether the observed neural interactions are genuine, and whether the observed connections are directed or modulated by an intermediate entity (Bastos and Schoffelen, 2016).

Volume conduction refers to the instantaneous spread of electrical currents through the conductive tissues surrounding an active neuronal source (Bastos and Schoffelen, 2016). In non-invasive recordings, a single source may be detected by multiple sensors, giving rise to spatial leakage: activity originating in one region "spills" into neighbouring channels, so that true regional signals are misattributed to adjacent areas. This leakage can produce entirely spurious functional connectivity estimates, since apparent coupling between two sensors may simply reflect their shared sensitivity to the same underlying source, rather than a genuine interaction between distinct neuronal populations (Bastos and Schoffelen, 2016).

Robust functional connectivity measures and source reconstruction techniques are proposed (Haufe et al., 2013; Nolte et al., 2004; Pellegrini et al., 2023) to overcome this issue. The robustness of the functional connectivity measures relies on the following assumption: volume conduction is instantaneous, meaning that if a source is picked up by two sensors simultaneously, the phase of the signals is the same (or a multiple of π). The usage of the imaginary part of coherency-based measures such as $\text{ImCOH}_{xy}(f)$, MIC, and PSI, is justified by this exact property. These measures ignore zero-phase lag interactions, which are assumed to be generated by volume conduction. However, not all zero-lag interactions are necessarily non-physiological (Gollo et al., 2014; Ossadtchi et al., 2018; Viriyopase et al., 2012). While such measures are blind to instantaneous zero-phase volume conduction artefacts, they also miss out on some portion of the true brain interactions with zero-phase or close to zero synchrony. While several techniques have been proposed to mitigate the spatial leakage effects, like symmetric orthogonalisation and multivariate leakage correction (Colclough et al., 2015), only the PSIICOS algorithm by Ossadtchi et al. (2018) allows the retention of true near-zero-lag synchrony. Nevertheless, robust functional connectivity measures provide satisfactory results capturing a large portion of the simulated functional and effective connections in the papers by Haufe et al. (2013) and Pellegrini et al. (2023).

Source reconstruction techniques project the sensor signals to the source space, allowing for the functional connectivity estimation between pairs of the estimated

sources instead of sensors. While it is a widely used technique frequently utilised in EEG/MEG imaging (Haufe et al., 2013; Pellegrini et al., 2023; Schoffelen and Gross, 2019), inverse operators are also contaminated by spatial leakage. Reconstructed signals still contain contributions from other neighbouring sources (Schoffelen and Gross, 2019). Additionally, this approach may lead to the propagation of time series estimation errors to the subsequent functional connectivity estimation. Nonetheless, existing research simulations analysing various analytical functional connectivity pipelines such as the ones by Haufe et al. (2013) and Pellegrini et al. (2023) demonstrate quite promising results.

Another problem that must be taken into consideration is the SNR problem. SNR is a measure used to quantify the level of a desired signal compared to the level of the background noise. The SNR problem follows partly as a result of the volume conduction problem since it emerges from the fact that the electrodes measure a mixture of signal-of-interest and noise (Bastos and Schoffelen, 2016). The noise component is composed of spatially incoherent brain noise and additive white noise (or sensor noise), which has a non-brain origin (Ossadtchi et al., 2018). Mathematically, SNR is expressed as the ratio of the power of the signal to the power of the noise. A higher SNR value indicates that the signal is stronger relative to the noise, and a lower SNR value signifies that the amount of noise exceeds the amount of the signal. Noisy signals with lower SNR obstruct the estimation of functional connectivity. Some consequences of the SNR problem include the spurious differences in functional connectivity between conditions, where the SNRs differ across conditions, and spurious differences in functional connectivity between signals that were observed under different SNRs (Bastos and Schoffelen, 2016). In the experimental setting, noise should be minimised as much as possible through the placement of the sensors that maximises the SNR (Bastos and Schoffelen, 2016). In the case when this approach is impossible, one could use the stratification technique (Bosman et al., 2012) to make the distributional properties of the signal power as similar to each other as possible (Bastos and Schoffelen, 2016).

Furthermore, the parameters of the analysed data, such as the ground-truth interactions, the noise composition, the length of the interaction delay, and the number of active sources per region, affect the performance of the analysing pipelines and, consequently, the functional connectivity estimation (Pellegrini et al., 2023).

In summary, although functional-connectivity estimation remains constrained

by volume conduction, spatial leakage, source-reconstruction error and variable SNR, these confounds can be substantially mitigated through robust connectivity metrics, careful source-space projection and rigorous experimental design. Systematic simulations (Haufe et al., 2013; Pellegrini et al., 2023) furnish quantitative benchmarks for pipeline performance, laying a firm foundation for the functional connectivity research presented in the next chapter.

Chapter 3. Materials and Methods

3.1 Hypotheses

Building on the PR framework and the oscillatory signatures reported by Hein et al. (2023), the present study examines differences in the frequency-specific functional connections between HTA and LTA participants during the reward-learning task under volatility performed by Hein et al. (2023). TRGC is employed as a robust measure of the statistical dependency between the sources, which may reflect directed information flow. The following hypotheses are tested:

1 In the late post-outcome interval, corresponding to the encoding of unsigned pwPEs of unexpected trials, HTA participants exhibit greater γ-band statistical dependency between the relevant sources compared to LTA participants;

Enhanced γ-band statistical dependency is anticipated because trait anxiety disrupts PC, yielding larger pwPEs when an outcome deviates from expectation and hence stronger γ signalling in higher cortical regions (Bastos et al., 2020; Gabhart et al., 2025; Hein et al., 2023). During the reward-learning task under volatility, this disruption should manifest as elevated γ-band statistical dependency between sources in HTA participants during the late post-outcome interval, reflecting faster belief updating (Hein et al., 2023).

2 In both the early and late post-outcome intervals, HTA participants exhibit reduced α/β-band statistical dependency between the sources of interest compared to LTA participants, reflecting enhanced feedforward γ activity at the expense of suppressed top-down α/β signalling.

The effects are expected in the cortical regions identified by Hein et al. (2023) as the key areas of disrupted PC in anxiety:

- Increased γ-band TRGC-connectivity in the ACC, dmPFC, and lOFC;
- Decreased α/β-band TRGC-connectivity in the ACC.

Trial "unexpectedness" is defined by the unsigned pwPEs estimated by the HGF (Hein et al., 2023), as described in the Section 3.4.3.

3.2 Participants

For the original study by Hein et al. (2023), 39 healthy adults were recruited (24 female, 15 male; mean age 22.8±0.9 years). All participants reported normal or corrected-to-normal vision and no previous neurological or psychiatric illness. Written informed consent was obtained from every volunteer, and the study by Hein et al. (2023) was approved by the ethics committee of the Institutional Review Board of the National Research University Higher School of Economics in Moscow, Russia.

3.2.1 State anxiety questionnaire. Participants were pre-screened using the trait subscale X2 of Spielberger's State-Trait Anxiety Inventory (STAI, 20 items, score 0-80, Spielberger, 1983) to form two groups: low trait anxiety (LTA; STAI $\leq$ 36) and high trait anxiety (HTA; STAI $\geq$ 45). These cut-offs were chosen to capture normative ($\leq$ 36) (Spielberger, 1983) and clinically elevated ($\geq$ 45) (Shadli et al., 2021) ranges of trait anxiety in non-clinical populations. STAI-T scores ranged between 24 and 65: mean 30.5±0.8 for LTA and mean 51.7±1.5 for HTA. Both groups were matched for age and sex (LTA: N = 20, 12 female; HTA: N = 19, 12 female). Based on the power analysis, a minimum of 16 participants per group was required (Hein et al., 2023), a criterion that was met. State anxiety was assessed twice: once immediately before participant selection and again at the start of the experiment.

3.3 MEG and MRI Acquisition

Neuromagnetic data were recorded continuously at a sampling rate of 1 kHz and band-pass filtered between 0.1 Hz and 330 Hz using a 306-channel Elekta Neuromag MEG system (102 magnetometers and 204 planar gradiometers). While participants, seated comfortably, carried out the experiment, eye movements and blinks were tracked with two horizontal and two vertical electrooculogram electrodes, and cardiac activity was measured through a pair of electrocardiography electrodes. Four HPI coils were used to monitor head position. After acquisition, the data were denoised and corrected for head motion with the Elekta MaxFilter software, employing the temporally extended signal-space algorithm (Taulu and Hari, 2009).

T1-weighted anatomical MRIs (1 mm^3, 1.5 T) were collected for source reconstruction in all participants in the original study. However, for the present study, the individual MRI scans were available for 34 participants. For the remaining five, the

coregistration of each subject's digitised head shape (scalp surface and fiducials) to the FreeSurfer fsaverage template was performed using MNE-Python's coregistration tools, as detailed in Section 3.4.2 below.

3.3.1 Experimental paradigm. Participants completed a probabilistic reversal-learning task comprising two blocks of 160 trials each (total 320 trials). On every trial, a blue and an orange fractal were presented (randomised left/right position); subjects had 1 300±125 ms to choose which stimulus they believed would yield reward (outcome win, 5 points; outcome lose = 0 points) by pressing a left or right button corresponding with the position of the fractal of their choice. Subjects were informed that their cumulative points would be converted to an additional monetary bonus at study end following the formula $(total\ points)/6 + 400$. The chosen fractal was highlighted for 1000±200 ms, followed by outcome feedback (win in green, lose or no response in red) for 1900±100 ms. Inter-trial intervals were presented for 1750±250 ms with the fixation cross in the centre of the screen (Figure 1).

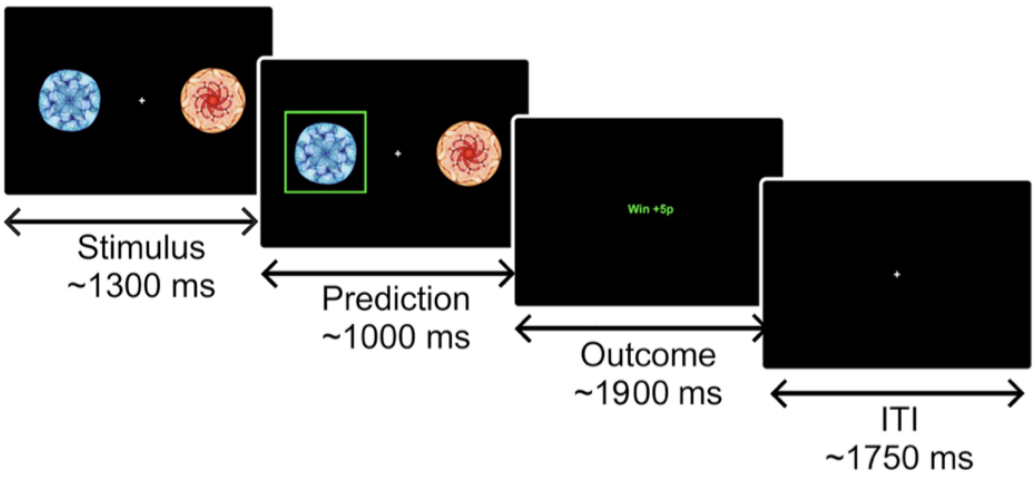

Figure 1: The structure of the behavioural task. Adapted from Hein et al., 2023.

Within each block, the reward contingency (probability that blue versus orange was rewarded) changed pseudorandomly every 26–38 trials, implementing four reversals per block. The five possible mappings per block were 0.9/0.1, 0.1/0.9, 0.7/0.3, 0.3/0.7, and 0.5/0.5 (win | blue / win | orange), counterbalanced across participants (see Hein et al. (2023) for more details).

3.4 Analysis Pipeline

The MEG data were preprocessed, source-reconstructed, and analysed for directed functional connectivity using TRGC as a measure of inter-regional statistical dependency, utilising a combination of MNE-Python (v1.9.0; Gramfort et al., 2013) and EEGLAB with the ROIconnect plugin (v2025.0.0; Pellegrini et al., 2023), with additional custom Python scripts (v3.12.2).

3.4.1 Preprocessing. Continuous recordings from magnetometers and planar gradiometers were preprocessed individually for each block. For two participants, only the second block recording was available for the analysis. First, the recordings were down-sampled to 250 Hz and notch-filtered at 50 Hz and its harmonics up to 300 Hz to eliminate power-line interference. Ocular and cardiac artefacts were identified and removed via independent component analysis (ICA, fastICA algorithm), with components flagged automatically and confirmed by visual inspection (mean components removed across two blocks: 3.8 ± 0.8). The data were then band-pass filtered between 1–40 Hz and epoched from -3s to +2s around outcome onset, when participants received feedback on their choice. Only these outcome epochs were retained for further analysis. The amplitude threshold was applied to reject noisy segments (5^{-12} T for magnetometers, 4^{-10} T/cm for gradiometers). One participant was excluded entirely at this stage due to excessive noise in both blocks. For the total number of epochs chosen for the analysis per participant after this preprocessing stage, see Table A1 in Appendix A.

3.4.2 Source reconstruction. The source reconstruction of MEG signals was carried out in MNE-Python using Linearly Constrained Minimum Variance (LCMV) beamforming (Van Veen et al., 1997). For 34 participants, individual T1-weighted MRIs were first processed in FreeSurfer 6.0 (Dale et al., 1999; Fischl et al., 1999) to generate surface-based cortical parcellations in each hemisphere by Hein et al. (2023). For the remaining five, each subject's digitised scalp surface and fiducial points were coregistered to the FreeSurfer fsaverage anatomy. Forward models were then computed on the fsaverage boundary-element model (BEM) surfaces (5120 triangles per layer) and the fsaverage-oct6 source space (8 196 vertices per hemisphere).

In all subjects, the data covariance was estimated from all outcome-locked epochs (0.05, 1.8s) and the noise covariance from a pre-stimulus baseline (-3, -2s)

using empirical covariance estimation. Uniform covariance regularisation (reg = 0.05) was applied, and LCMV filters were computed with unit-noise-gain normalisation and maximal-power orientation selection. Conceptually, this procedure designs spatial filters that maximise activity from each target location with minimal variance in all other directions, yielding optimal source time series while suppressing interference from non-target regions.

Source-reconstructed time series were then extracted from cortical labels defined by the Desikan–Killiany (DK) atlas (Desikan et al., 2006) using the `pca_flip` method in MNE-Python. For each trial and each label, PCA was performed on the source-space time samples and the dominant component's polarity was aligned to ensure consistency across trials. Although the flip operator does not affect spectral amplitude estimates, it is essential for producing phase-coherent time series suitable for directed connectivity analysis (Ivanova et al., 2025). Finally, the extracted source-reconstructed activity was averaged within 13 bilateral ROIs; however, for the subsequent connectivity estimation, only 7 bilateral ROIs implicated in decision-making under uncertainty and reward processing (Grupe and Nitschke, 2013; Hein et al., 2023; Paulus et al., 2004; E. T. Rolls et al., 2022; Schulreich and Schwabe, 2021) were selected. These include 1. ACC, 2. OFC (including vmPFC), 3. dmPFC, 4. dlPFC. The correspondence between these regions and their DK labels is given in Table 1.

Table 1: Desikan–Killiany labels grouped by cortical region

Region	DK labels	Labels
ACC	caudal and rostral ACC	4
OFC (including vmPFC)	lateral and medial OFC	4
dmPFC	superior frontal gyrus	2
dlPFC	caudal and rostral MFG	4
Total		14

Notes. ACC = anterior cingulate cortex; OFC = orbitofrontal cortex; vmPFC = ventromedial prefrontal cortex; dmPFC = dorsomedial prefrontal cortex; dlPFC = dorsolateral prefrontal cortex

3.4.3 Connectivity analysis. Source-reconstructed time series were organised into single trials and combined with each participant's unsigned pwPEs derived from the HGF model from Hein et al. (2023). To isolate unexpected trials associated with

faster belief updating, a medial split was applied to each participant's distribution of unsigned pwPEs, retaining those trials with values above the median for the analysis.

The directionality of the information flow among our 14 DK ROIs was estimated using a robust measure of statistical dependency, TRGC, via the ROIconnect EEGLAB plugin (Pellegrini et al., 2023). The TRGC spectra were computed over two successive post-outcome intervals, early (0–0.5 s) and late (0.5–1 s), to separately capture initial error signalling and the subsequent belief-updating. To focus the analyses on the oscillatory components most relevant to the PR framework, the TRGC values were then averaged within four frequency bands, each selected for its specific functional role in hierarchical inference and according to the hypotheses of the study (see Section 3.1):

- θ (4–7 Hz): part of the exploratory analysis based on its putative role in PR according to Bastos et al. (2020);
- α (8–12 Hz) and β (13–30 Hz): indexing top-down and the maintenance versus revision of internal models following unexpected outcomes;
- γ (32–100 Hz): indexing feedforward PE signalling under the PR model and reflecting rapid updating of cortical representations (Bastos et al., 2020).

3.5 Statistical Analysis

Resulting TRGC matrices (shape $n_F \times n_{\mathrm{ROI}} \times n_{\mathrm{ROI}}$, with n_F frequency bins and $n_{\mathrm{ROI}} = 14$ DK-labelled ROIs) were averaged over four predefined frequency bands and two predefined post-outcome intervals (early and late).

Between-group comparisons (HTA versus LTA) for each band $\times$ interval $\times$ $n_{\mathrm{ROI}} \times n_{\mathrm{ROI}}$ connections were performed using non-parametric permutation tests (`permutation_test` from SciPy, v1.15.2) with 10000 randomisations. The test statistic T_{ij} was the difference of mean TRGC values between the groups:

$$T_{ij} = \overline{r}_{ij}^{\mathrm{HTA}} - \overline{r}_{ij}^{\mathrm{LTA}},$$

where $\overline{r}_{ij}^{G}$ is the average over N_G subjects in group $G \in \{\mathrm{HTA}, \mathrm{LTA}\}$ for a given pair of ROIs (i, j). Two-sided tests were used for exploratory analyses in the θ range; when a specific directional hypothesis was formulated (for example, increase in γ-band statistical dependency in HTA participants), one-sided tests were employed

with the alternative hypothesis specified accordingly (for example, for HTA>LTA, we specify `alternative='greater'`). All tests were conducted at an uncorrected $\alpha = 0.05$. To control for the large number of pairwise comparisons, p-values were adjusted using the Benjamini–Hochberg false discovery rate (FDR) (Benjamini and Hochberg, 1995) procedure ($q = 0.05$). Statistically significant connections are reported at FDR-corrected p-values < 0.05.

3.6 Results

All inferential statistics reported below survive FDR-correction across all tested $n_{\text{ROI}} \times n_{\text{ROI}}$ connections. Uncorrected p-value matrices for θ, α, and β frequency bands for both time intervals are provided in Appendix B.

In all TRGC-spectra figures, the HTA group is shown in **blue** and the LTA group in **green**. The shaded ribbon around each trace denotes the standard error of the mean, computed as the across-subjects standard deviation divided by $\sqrt{N}$. A light grey vertical band highlights the frequency band of interest; all reported p-values refer to tests on the average TRGC within this band. The x-axis gives frequency in Hz, and the y-axis shows TRGC values, which quantify the statistical dependency between ROIs: their magnitude corresponds to the coupling strength, and their sign indicates the predominant direction of influence. Each panel title names the connection as TRGC: "Region$_1$ to Region$_2$, p-value k", where k is the FDR-corrected p-value for that connection. Regions are abbreviated as follows:

- a prefix {l, m, c, r} for lateral, medial, caudal, or rostral;
- one of {MFG, OFC, ACC} for middle frontal gyrus, orbitofrontal cortex, or anterior cingulate cortex;
- and a final “l” or “r” indicating left or right hemisphere.

Thus, "cMFGl to rMFGr" denotes the directed statistical dependency between the the left caudal MFG to the right rostral MFG.

3.6.1 γ-band connectivity: late post-outcome interval. For the γ-band connections, it was hypothesised that HTA participants would exhibit enhanced statistical dependencies between sources during the encoding of pwPEs compared to LTA participants. Figure 2b shows the FDR-corrected p-value matrix for all γ-band

connections in the late post-outcome time interval (Figure 2a shows the uncorrected p-value matrix). Two connections were characterised by significantly greater statistical dependency in HTA compared to LTA:

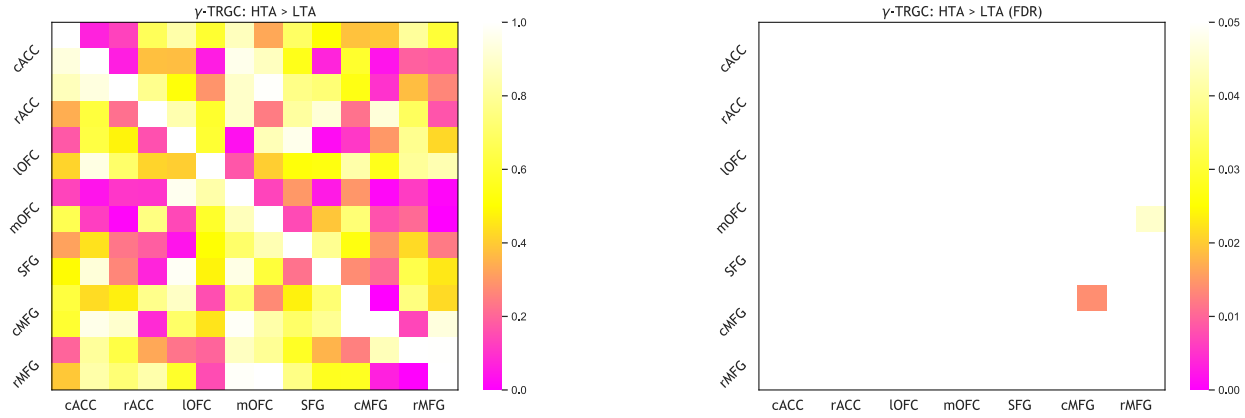

(a) Uncorrected p-value matrix

(b) FDR-corrected p-value matrix

Figure 2: P-value matrices for γ-band connections in the late post-outcome interval. In *a).* white cells denote $p_{\text{uncor}} \geq 1$, while white cells in *b).* denote $p_{\text{FDR}} \geq 0.05$

1 From the left cMFG to the right cMFG; $p_{\text{FDR}} = 0.014$ (Figure 3a);

2 From the right mOFC to the right rMFG, $p_{\text{FDR}} = 0.0448$ (Figure 3b).

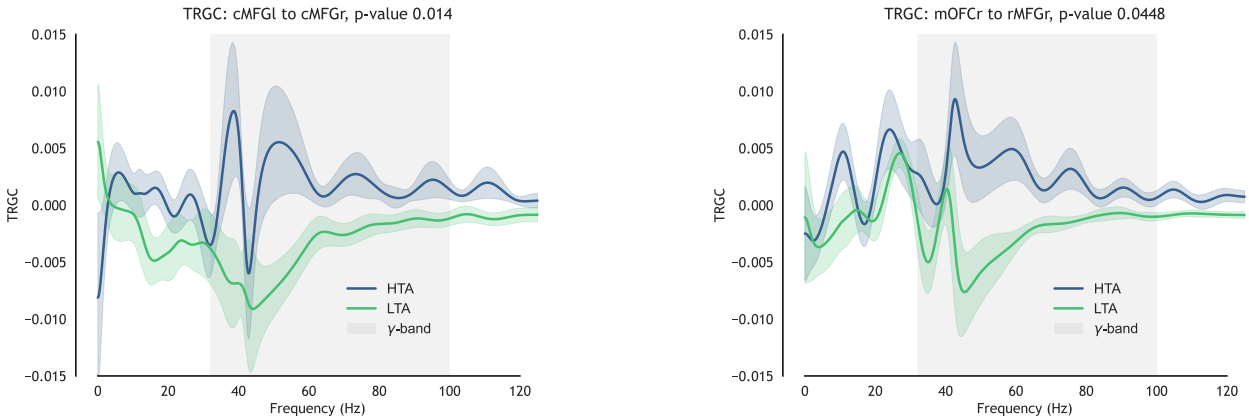

(a) Caudal MFG (L) → Caudal MFG (R), $p_{\text{FDR}} = 0.014$

(b) Medial OFC (R) → Rostral MFG (R), $p_{\text{FDR}} = 0.0448$

Figure 3: Significant between-group TRGC effects in the γ-band during the late post-outcome interval.

3.6.2 α/β-band connectivity: late post-outcome interval. For the connections in the α/β frequency range, it was hypothesised that HTA participants would

exhibit decreased statistical dependencies between ROIs during both early and late time intervals in HTA compared to LTA, allowing the γ-band signalling to encode pwPEs. No α/β connections reached significance in the early post-outcome time interval (see Figures B2 and B3 for the uncorrected p-value matrices). However, during the late interval (Figure 4), each frequency band revealed a single connection in which HTA participants exhibited significantly decreased statistical dependency compared to LTA:

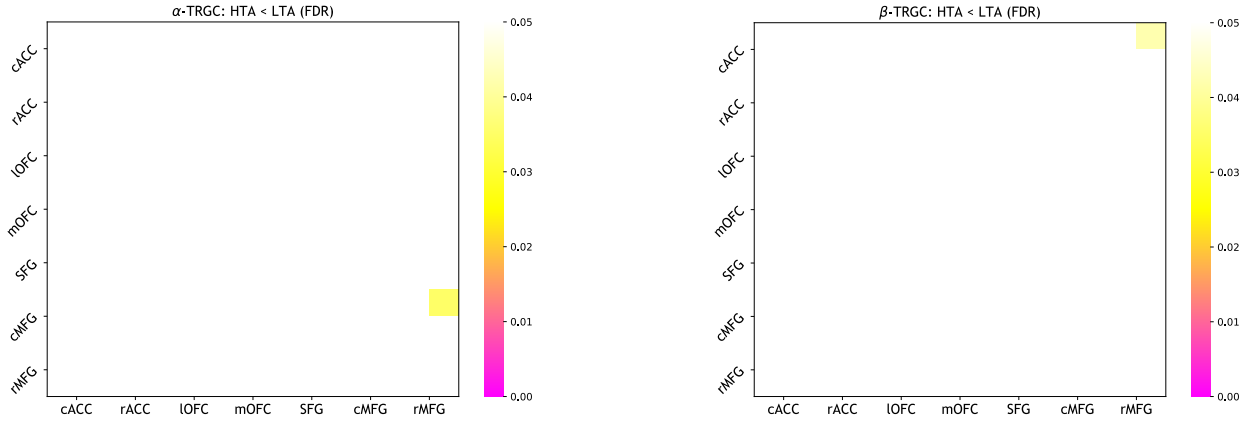

(a) α frequency range

(b) β frequency range

Figure 4: FDR-corrected p-value matrices for α/β-band connections in the late post-outcome interval. White cells denote $p_{\text{FDR}} \geq 0.05$.

1 α-band range: from the left cMFG to the right rMFG, $p_{\text{FDR}} = 0.035$ (Figure 5a);

2 β-band range: from the left cACC to the right rMFG, $p_{\text{FDR}} = 0.042$ (Figure 5b).

3.6.3 Exploratory θ-band connectivity: early post-outcome interval. Because no a prior hypothesis was specified for the θ-band statistical dependency differences between the groups, all tests were two-sided.

1 In the early post-outcome interval, one connection from the right lOFC to the left mOFC exhibited statistically significant increase of statistical dependency in HTA compared to LTA, $p_{\text{FDR}} = 0.0476$ (Figure 6);

2 In the late post-outcome interval, no connections survived the FDR correction (see Figure B1 for the uncorrected p-value matrices).

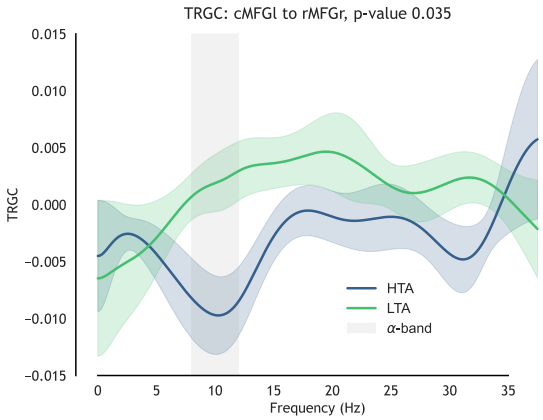

(a) Caudal MFG (L) → Rostral MFG (R), $p_{\text{FDR}} = 0.035$

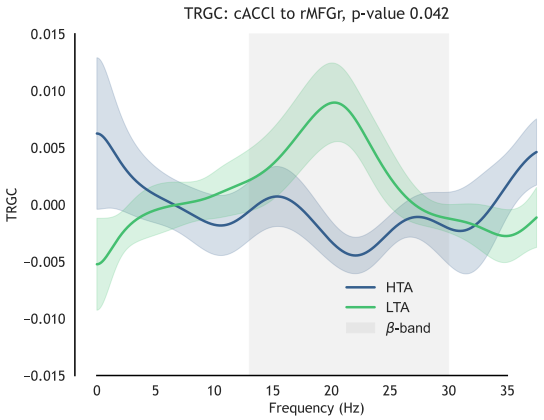

(b) Caudal ACC (L) → Rostral MFG (R), $p_{\text{FDR}} = 0.042$

Figure 5: Significant between-group TRGC effects in the α- (left) and β- (right) bands during the late post-outcome interval.

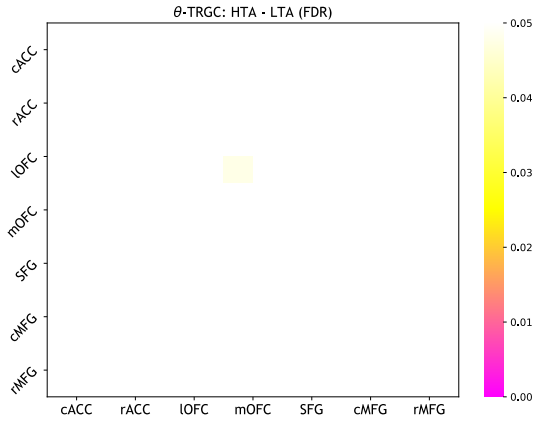

(a) FDR-corrected p-value matrix

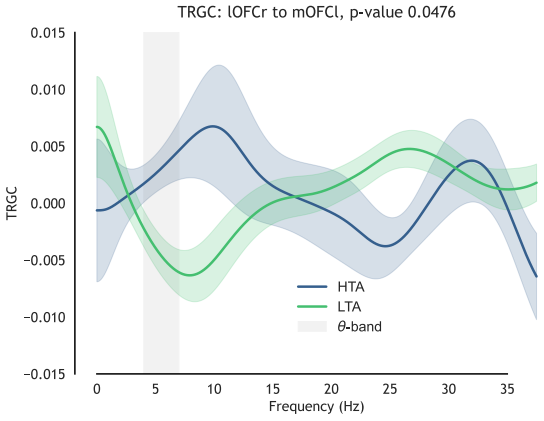

(b) Lateral OFC (R) → Medial OFC (L), $p = 0.0476$

Figure 6: θ-band statistical dependency in the early post-outcome interval: *a)*. FDR-corrected p-value matrix, where white cells denote $p_{\text{FDR}} \geq 0.05$, and *b)*. significant between-group TRGC effects.

Overall, across all frequency bands and post-outcome intervals, only a small number of prefrontal connections survived FDR correction: two in the γ-band, one in the α-band and one in the β-band, with one in the early-θ time window. Moreover, these effects were confined to just five cortical loci: lateral and medial OFC, rostral and caudal MFG, and caudal ACC. No additional connections reached FDR-corrected significance.

Chapter 4. Summary and Discussion

This chapter interprets the connectivity results presented in Section 3.6 in the context of previous work on anxiety-related network alterations (Section 2.1) and rhythm-specific predictive coding (Section 2.2). For clarity, Table 2 lists all statistically significant FDR-corrected statistical dependency effects for the HTA group alongside their putative functional roles.

Table 2: Directed connections that survived FDR correction

Window	Connection	Effect & Role
Early, θ	right lOFC $\rightarrow$ left mOFC	$\uparrow$ relay of volatility signals
Late, γ	right mOFC $\rightarrow$ right rMFG	$\uparrow$ feed-forward pwPE propagation
Late, γ	left cMFG $\rightarrow$ right cMFG	$\uparrow$ feed-forward pwPE propagation
Late, α	left cMFG $\rightarrow$ right rMFG	$\downarrow$ top-down control
Late, β	left cACC $\rightarrow$ right rMFG	$\downarrow$ uncertainty modulation

Notes. The Window column combines the post-outcome time interval (early = 0-0.5s, late = 0.5-1s) with the frequency at which the between-group difference reached FDR-corrected significance. The Effect & Role column uses $\uparrow$ to denote increased statistical dependency in HTA versus LTA and $\downarrow$ to denote decreased statistical dependency, followed by the putative functional role

4.1 Relationship to Known Anxiety Circuitry

Early θ exchange between lateral and medial OFC. Hein et al. (2023) demonstrated that HTA participants overestimate environmental volatility and express larger outcome-related γ-band responses in the lOFC. The early θ-band connection (Section 3.6.3) from the right lOFC to the left mOFC may suggest that the this "volatility detector" is relayed almost immediately to the mOFC, a region implicated in encoding the reward value and in the "uncertainty and anticipation model of anxiety" (Grupe and Nitschke, 2013; Hein et al., 2023).

Right rMFG as a convergence hub. In HTA participants, connections to the right rMFG exhibit the opposing patterns of statistical dependency: this region receives suppressed α/β signalling but enhanced γ input (see Table 2). This rhythm-specific imbalance aligns with the PR framework (Bastos et al., 2020), in which deep-layer α/β-band signalling conveys top-down predictions, whereas superficial γ oscillations carry bottom-up PEs. In HTA, suppressed α/β amplitude (as shown by Hein et

al. (2023)) and decreased statistical dependency may allow enhanced γ-band error signalling to alter executive processing in the right rMFG (dlPFC), which is heavily involved in decision-making and action selection (Grupe and Nitschke, 2013).

Altered β-band control from cACC. The DK-labelled cACC corresponds to a region referred to as the dorsal anterior cingulate or anterior midcingulate cortex (aMCC) (Delfin et al., 2021; Heilbronner and Hayden, 2016), which is said to be involved in the probability assessment (Grupe and Nitschke, 2013). The suppression of β-band statistical dependency between the left cACC and the right rMFG (Section 3.6.2) echoes the reduced α/β-band power in the cACC during pwPE encoding in HTA participants reported by Hein et al. (2023). Such patterns of altered statistical dependency between the aMCC and other frontal regions, including the dlPFC, may undermine the selection of appropriate responses to uncertainty (Grupe and Nitschke, 2013).

Left cMFG as a rhythm switch. Left cMFG (dlPFC) may act as a "rhythm switch": it exhibits reduced α/β-band statistical dependency to the right rMFG while simultaneously enhancing γ-band statistical dependency, that corresponds to the encoding of PEs, to the right cMFG (Sections 3.6.2 and 3.6.1).

Belief-updating signals localised to posterior MFG in the fMRI study by Kobayashi and Hsu (2017) have been shown to drive ipsilateral vmPFC under reducing uncertainty. Similarly, the current finding of the late γ-signalling from the left cMFG to its right-hemisphere homologue may establish cMFG as the driver of the update signalling. A separate γ-band connection from the right mOFC to the ipsilateral rMFG may may, therefore, indicate that valuation-related mOFC forwards pwPEs to MFG for executive use.

4.2 Implications of the Findings

The connectivity results refine the understanding that trait anxiety is characterised by stronger PE signalling and a rhythm-specific imbalance. Weak α/β-band statistical dependency between the cACC and rMFG fails to dampen frontal belief-updating by inhibiting γ-band PE signalling. In the Bayesian PC terms, it biases the system to attach more precision to the incoming PE signalling. As precision is encoded in terms of the α/β-band signalling (Hein et al., 2023), the suppression of

these oscillations leads to the overweighting of precision, behaviourally manifested as more stochastic choices and lose-shift tendencies (Hein et al., 2023).

Certain Hein et al. (2023) findings did not re-emerge in the present study:

1. No γ-band statistical dependency arising in the ACC was identified, while Hein et al. (2023) reported enhanced γ-band responses in the cACC during the encoding of unsigned pwPEs;

2. No early α/β-band effects were identified, while both early and late α/β modulations were identified in Hein et al. (2023) in the cACC, lOFC, and superior frontal gyrus (SFG);

3. No statistical dependency for the dmPFC (SFG) was implicated, while the dmPFC showed strong γ-band effects in Hein et al. (2023).

A plausible explanation for these discrepancies may lie in the methodological focus of the present study on the directed inter-regional statistical dependencies. Increases in local oscillatory power, such as those described by Hein et al. (2023), may not necessarily translate into stronger long-range dependencies (Hindriks and Tewarie, 2023). Phase-based coupling between distant cortical areas typically builds up over multiple oscillatory cycles; they may, therefore, extend beyond the temporal intervals examined in the present study (Akam and Kullmann, 2012; Fries, 2015; Lachaux et al., 1999). Examining a later post-outcome interval ($\geq$1 s) could elucidate whether delayed statistical dependency emerges and reconciles these two sets of findings.

Since anxiety is associated with disruptions in the synchronisation and activation of several large-scale networks and diverse subcortical structures (see Section 2.1), such as the amygdala, dorsomedial thalamus, insular cortex, pallidum, and hippocampus, it is advantageous to employ multimodal approaches when characterising the neural activity underlying this condition. Most investigations of state anxiety have relied on a single neuroimaging modality, for example, fMRI (De la Peña-Arteaga et al., 2024; Geng et al., 2018; Saviola et al., 2020), MEG (Hein et al., 2023;), or EEG (Berchio et al., 2019; Cheng et al., 2025; Hein et al., 2021; Imperatori et al., 2019; Ioakeimidis et al., 2023; Knyazev et al., 2004). Combining the high spatial resolution of fMRI with the millisecond temporal precision of MEG may, however, yield additional explanatory power and provide deeper insight into the spatiotemporal dynamics

of anxious learning. Multimodal integration allows for the combination of different data types to obtain a more nuanced picture of the brain functioning (Baghdadi et al., 2025). While this integration inevitably complicates the experimental workflow and analytical pipeline, it is worth investigating the potential scientific benefits; for example, Cetin et al. (2016) demonstrated that joint fMRI-MEG features led to an improvement in the classification of schizophrenia, a disorder likewise characterised by aberrant oscillatory activity and functional connectivity.

Chapter 5. Conclusion

Trait anxiety is a stable disposition that biases individuals towards threat overestimation and adopting negative expectations about future events. High-trait-anxious (HTA) people fall into the subclinical anxiety group with higher risks for affective disorders, and even in the absence of a clinical diagnosis, affected individuals suffer measurable consequences: they switch choices more readily after losses, learn less efficiently, and ultimately perform worse than their low-trait-anxious (LTA) peers. To reveal the neural circuitry that may drive this behavioural profile, the present study aimed to determine the frequency-specific functional connectivity differences between HTA and LTA individuals during reward-based learning under environmental volatility. Building on top of the predictive routing framework and oscillatory signatures of reversal learning in anxiety under uncertainty identified by Hein et al. (2023), we hypothesised that HTA individuals would exhibit enhanced γ-band statistical dependencies between frontal regions involved in decision-making and reward processing, such as the OFC, ACC, dlPFC, and dmPFC. This increase was expected to occur during the encoding of prediction errors, which is governed by feedforward γ oscillation in the superficial cortical layers. On the contrary, the γ power increase is accompanied by the decrease in α/β power; thus, we hypothesised that HTA individuals would exhibit suppressed α/β-band statistical dependencies between the regions of interest, mainly arising in ACC, before and during the encoding of prediction errors. Statistical dependency between regions in the θ-band was a part of the exploratory analysis.

In order to check the hypotheses, we combined MEG source reconstruction with Time-reversed Granger causality estimation of directed inter-regional statistical dependencies arising during belief updating, which was identified based on the Hierarchical Gaussian Filter model assessing the precision-weighted prediction errors. The results of the non-parametric permutation testing with the multiple comparisons correction partially support our hypotheses. HTA individuals displayed enhanced γ-band statistical dependencies within a fronto-cortical network that encompasses caudal ACC, dlPFC, and lateral and medial parts of OFC. Concurrently, HTA individuals exhibited suppressed α/β-band statistical dependency between ACC and dlPFC, supporting the predictive routing account of anxious learning. An early θ-band connection interhemispherically linking lateral and medial parts of OFC,

suggesting that θ-band oscillations may be involved in the transmission of volatility signals for further valuation. However, there were no early α/β-band statistical dependencies, and the dmPFC was not recruited during prediction-error encoding, as it was expected following the amplitude findings by Hein et al. (2023). A likely explanation is that local amplitude changes do not necessarily propagate into long-range statistical dependencies. Additionally, they may not emerge in the time interval analysed in the present study.

Together, the current findings confirm the rhythm-specific nature of the predictive routing framework and refine its account of anxiety: suppressed α/β signalling from cACC and cMFG may allow enhanced γ prediction-error signalling to influence the decision-making in the dlPFC. Behaviourally, this manifests as an inflated sense of environmental volatility, heavier weighting of prediction errors, more stochastic choices, and poorer overall performance. By linking computational theories of uncertainty to alterations in large-scale network statistical dependency, this mechanistic account helps explain everyday decision-making impairments observed in HTA individuals.

Limitations include the focus on earlier (< 1 s) post-outcome intervals and cortical sources only due to the nature of MEG. Future work should therefore 1. examine later time intervals to track the evolution of statistical dependencies, 2. integrate multimodal (MEG-fMRI) approaches to capture deep-layer and subcortical dynamics, and 3. test whether the identified rhythm-specific signatures can serve as biomarkers for intervention or prediction of clinical conversion.

In sum, the study confirms that state anxiety disrupts predictive routing: suppressed α/β feedback and enhanced γ feedforward signalling translate trait anxiety into maladaptive learning and behaviour.

References

Abbott, L. F., Bock, D. D., Callaway, E. M., Denk, W., Dulac, C., Fairhall, A. L., Fiete, I., Harris, K. M., Helmstaedter, M., Jain, V., Kasthuri, N., LeCun, Y., Lichtman, J. W., Littlewood, P. B., Luo, L., Maunsell, J. H. R., Reid, R. C., Rosen, B. R., Rubin, G. M., . . . Essen, D. C. V. (2020). The Mind of a Mouse. *Cell*, *182*(6), 1372–1376. https://doi.org/10.1016/j.cell.2020.08.010

Abdallah, C. G., Averill, C. L., Ramage, A. E., Averill, L. A., Goktas, S., Nemati, S., Krystal, J. H., Roache, J. D., Resick, P. A., Young-McCaughan, S., Peterson, A. L., & Fox, P. (2019). Salience Network Disruption in U.S. Army Soldiers With Posttraumatic Stress Disorder. *Chronic Stress*, *3*, 2470547019850467. https://doi.org/10.1177/2470547019850467

Akam, T. E., & Kullmann, D. M. (2012). Efficient "communication through coherence" requires oscillations structured to minimize interference between signals. *PLoS computational biology*, *8*(11), e1002760. https://doi.org/10.1371/journal.pcbi.1002760

American Psychiatric Association. (2022). *Diagnostic and Statistical Manual of Mental Disorders, Text Revision Dsm-5-tr* (5th edition). Amer Psychiatric Pub Inc.

Ardila, A., Bernal, B., & Rosselli, M. (2015). Language and Visual Perception Associations: Meta-Analytic Connectivity Modeling of Brodmann Area 37. *Behavioural Neurology*, *2015*, e565871. https://doi.org/10.1155/2015/565871

Baghdadi, G., Hadaeghi, F., & Kamarajan, C. (2025). Editorial: Multimodal approaches to investigating neural dynamics in cognition and related clinical conditions: Integrating EEG, MEG, and fMRI data. *Frontiers in Systems Neuroscience*, *19*. https://doi.org/10.3389/fnsys.2025.1495018

Bassett, D. S., & Gazzaniga, M. S. (2011). Understanding complexity in the human brain. *Trends in Cognitive Sciences*, *15*(5), 200–209. https://doi.org/10.1016/j.tics.2011.03.006

Bassett, D. S., Zurn, P., & Gold, J. I. (2018). On the nature and use of models in network neuroscience. *Nature Reviews Neuroscience*, *19*(9), 566–578. https://doi.org/10.1038/s41583-018-0038-8

Bastos, A. M., Vezoli, J., & Fries, P. (2015). Communication through coherence with inter-areal delays. *Current Opinion in Neurobiology*, *31*, 173–180. https://doi.org/10.1016/j.conb.2014.11.001

Bastos, A. M., Lundqvist, M., Waite, A. S., Kopell, N., & Miller, E. K. (2020). Layer and rhythm specificity for predictive routing. *Proceedings of the National Academy of Sciences of the United States of America*, *117*(49), 31459–31469. https://doi.org/10.1073/pnas.2014868117

Bastos, A. M., & Schoffelen, J.-M. (2016). A Tutorial Review of Functional Connectivity Analysis Methods and Their Interpretational Pitfalls. *Frontiers in Systems Neuroscience*, *9*. https://doi.org/10.3389/fnsys.2015.00175

Bateson, M., Brilot, B., & Nettle, D. (2011). Anxiety: An Evolutionary Approach. *The Canadian Journal of Psychiatry*, *56*(12), 707–715. https://doi.org/10.1177/070674371105601202

Bayraktaroglu, Z., von Carlowitz-Ghori, K., Losch, F., Nolte, G., Curio, G., & Nikulin, V. V. (2011). Optimal imaging of cortico-muscular coherence through a novel regression technique based on multi-channel EEG and un-rectified EMG. *NeuroImage*, *57*(3), 1059–1067. https://doi.org/10.1016/j.neuroimage.2011.04.071

Benjamini, Y., & Hochberg, Y. (1995). Controlling the False Discovery Rate: A Practical and Powerful Approach to Multiple Testing. *Journal of the Royal Statistical Society Series B: Statistical Methodology*, *57*(1), 289–300. https://doi.org/10.1111/j.2517-6161.1995.tb02031.x

Berchio, C., Rodrigues, J., Strasser, A., Michel, C. M., & Sandi, C. (2019). Trait anxiety on effort allocation to monetary incentives: A behavioral and high-density EEG study. *Translational Psychiatry*, *9*(1), 1–13. https://doi.org/10.1038/s41398-019-0508-4

Bishop, S. J. (2007). Neurocognitive mechanisms of anxiety: An integrative account. *Trends in Cognitive Sciences*, *11*(7), 307–316. https://doi.org/10.1016/j.tics.2007.05.008

Bosman, C. A., Schoffelen, J.-M., Brunet, N., Oostenveld, R., Bastos, A. M., Womelsdorf, T., Rubehn, B., Stieglitz, T., De Weerd, P., & Fries, P. (2012). Attentional stimulus selection through selective synchronization between monkey visual areas. *Neuron*, *75*(5), 875–888. https://doi.org/10.1016/j.neuron.2012.06.037

Brookes, M. J., Gibson, A. M., Hall, S. D., Furlong, P. L., Barnes, G. R., Hillebrand, A., Singh, K. D., Holliday, I. E., Francis, S. T., & Morris, P. G. (2004). A general linear model for MEG beamformer imaging. *NeuroImage*, *23*(3), 936–946. https://doi.org/10.1016/j.neuroimage.2004.06.031

Browning, M., Behrens, T. E., Jocham, G., O'Reilly, J. X., & Bishop, S. J. (2015). Anxious individuals have difficulty learning the causal statistics of aversive environments. *Nature Neuroscience*, *18*(4), 590–596. https://doi.org/10.1038/nn.3961

Buzsáki, G. (2006). *Rhythms of the Brain* (Illustrated). Oxford University Press.

Cannon, J., McCarthy, M. M., Lee, S., Lee, J., Börgers, C., Whittington, M. A., & Kopell, N. (2014). Neurosystems: Brain rhythms and cognitive processing. *European Journal of Neuroscience*, *39*(5), 705–719. https://doi.org/10.1111/ejn.12453

Carleton, R. N., Mulvogue, M. K., Thibodeau, M. A., McCabe, R. E., Antony, M. M., & Asmundson, G. J. G. (2012). Increasingly certain about uncertainty: Intolerance of uncertainty across anxiety and depression. *Journal of Anxiety Disorders*, *26*(3), 468–479. https://doi.org/10.1016/j.janxdis.2012.01.011

Cetin, M. S., Houck, J. M., Rashid, B., Agacoglu, O., Stephen, J. M., Sui, J., Canive, J., Mayer, A., Aine, C., Bustillo, J. R., & Calhoun, V. D. (2016). Multimodal Classification of Schizophrenia Patients with MEG and fMRI Data Using Static and Dynamic Connectivity Measures. *Frontiers in Neuroscience*, *10*. https://doi.org/10.3389/fnins.2016.00466

Cheng, C.-H., Chan, P.-Y. S., Chen, S.-Y., Chen, Y.-H., Lu, H., & Liu, C.-Y. (2025). Trait anxiety negatively modulates the coupling of motor event-related desynchronization and event-related synchronization. *BMC Psychiatry*, *25*(1), 447. https://doi.org/10.1186/s12888-025-06901-5

Clark, A. (2013). Whatever next? Predictive brains, situated agents, and the future of cognitive science. *Behavioral and Brain Sciences*, *36*(3), 181–204. https://doi.org/10.1017/S0140525X12000477

Cohen, M. X., Heller, A. S., & Ranganath, C. (2005). Functional connectivity with anterior cingulate and orbitofrontal cortices during decision-making. *Cognitive Brain Research*, *23*(1), 61–70. https://doi.org/10.1016/j.cogbrainres.2005.01.010

Cohen, M. X. (2015). Effects of time lag and frequency matching on phase-based connectivity. *Journal of Neuroscience Methods*, *250*, 137–146. https://doi.org/10.1016/j.jneumeth.2014.09.005

Cohen, M. X. (2014). *Analyzing Neural Time Series Data: Theory and Practice*. The MIT Press. https://doi.org/10.7551/mitpress/9609.001.0001

Colclough, G. L., Brookes, M. J., Smith, S. M., & Woolrich, M. W. (2015). A symmetric multivariate leakage correction for MEG connectomes. *NeuroImage*, *117*, 439–448. https://doi.org/10.1016/j.neuroimage.2015.03.071

Coutinho, J. F., Fernandesl, S. V., Soares, J. M., Maia, L., Gonçalves, Ó. F., & Sampaio, A. (2016). Default mode network dissociation in depressive and anxiety states. *Brain Imaging and Behavior*, *10*(1), 147–157. https://doi.org/10.1007/s11682-015-9375-7

Dale, A. M., Fischl, B., & Sereno, M. I. (1999). Cortical Surface-Based Analysis: I. Segmentation and Surface Reconstruction. *NeuroImage*, *9*(2), 179–194. https://doi.org/10.1006/nimg.1998.0395

de Berker, A. O., Rutledge, R. B., Mathys, C., Marshall, L., Cross, G. F., Dolan, R. J., & Bestmann, S. (2016). Computations of uncertainty mediate acute stress responses in humans. *Nature Communications*, *7*(1), 10996. https://doi.org/10.1038/ncomms10996

De la Peña-Arteaga, V., Chavarría-Elizondo, P., Juaneda-Seguí, A., Martínez-Zalacaín, I., Morgado, P., Menchón, J. M., Picó-Pérez, M., Fullana, M. A., & Soriano-Mas, C. (2024). Trait anxiety is associated with attentional brain networks. *European Neuropsychopharmacology*, *83*, 19–26. https://doi.org/10.1016/j.euroneuro.2024.02.013

Delfin, C., Andiné, P., Wallinius, M., & Björnsdotter, M. (2021). Structural Brain Correlates of the Externalizing Spectrum in Young Adults. *Neuroscience*, *463*, 1–13. https://doi.org/10.1016/j.neuroscience.2021.03.018

Dennett, D. C. (1997). *Kinds Of Minds: Toward An Understanding Of Consciousness* (Illustrated edition). Basic Books.

Deshpande, G., Hu, X., Stilla, R., & Sathian, K. (2008). Effective connectivity during haptic perception: A study using Granger causality analysis of functional magnetic resonance imaging data. *NeuroImage*, *40*(4), 1807–1814. https://doi.org/10.1016/j.neuroimage.2008.01.044

Desikan, R. S., Ségonne, F., Fischl, B., Quinn, B. T., Dickerson, B. C., Blacker, D., Buckner, R. L., Dale, A. M., Maguire, R. P., Hyman, B. T., Albert, M. S., & Killiany, R. J. (2006). An automated labeling system for subdividing the human cerebral cortex on MRI scans into gyral based regions of interest. *NeuroImage*, *31*(3), 968–980. https://doi.org/10.1016/j.neuroimage.2006.01.021

Diaconescu, A. O., Mathys, C., Weber, L. A. E., Daunizeau, J., Kasper, L., Lomakina, E. I., Fehr, E., & Stephan, K. E. (2014). Inferring on the Intentions of Others by Hierarchical Bayesian Learning. *PLOS Computational Biology*, *10*(9), e1003810. https://doi.org/10.1371/journal.pcbi.1003810

Dugger, B. N., & Dickson, D. W. (2017). Pathology of Neurodegenerative Diseases. *Cold Spring Harbor Perspectives in Biology*, *9*(7), a028035. https://doi.org/10.1101/cshperspect.a028035

Ewald, A., Marzetti, L., Zappasodi, F., Meinecke, F. C., & Nolte, G. (2012). Estimating true brain connectivity from EEG/MEG data invariant to linear and static transformations in sensor space. *NeuroImage*, *60*(1), 476–488. https://doi.org/10.1016/j.neuroimage.2011.11.084

Feldman, H., & Friston, K. (2010). Attention, Uncertainty, and Free-Energy. *Frontiers in Human Neuroscience*, *4*. https://doi.org/10.3389/fnhum.2010.00215

Fischl, B., Sereno, M. I., & Dale, A. M. (1999). Cortical Surface-Based Analysis: II: Inflation, Flattening, and a Surface-Based Coordinate System. *NeuroImage*, *9*(2), 195–207. https://doi.org/10.1006/nimg.1998.0396

Fries, P. (2015). Rhythms For Cognition: Communication Through Coherence. *Neuron*, *88*(1), 220–235. https://doi.org/10.1016/j.neuron.2015.09.034

Friston, K., & Kiebel, S. (2009). Predictive coding under the free-energy principle. *Philosophical Transactions of the Royal Society B: Biological Sciences*, *364*(1521), 1211–1221. https://doi.org/10.1098/rstb.2008.0300

Friston, K. J. (2011). Functional and Effective Connectivity: A Review. *Brain Connectivity*, *1*(1), 13–36. https://doi.org/10.1089/brain.2011.0008

Gabhart, K. M., Xiong, Y. (, & Bastos, A. M. (2025). Predictive coding: A more cognitive process than we thought? *Trends in Cognitive Sciences*, *0*(0). https://doi.org/10.1016/j.tics.2025.01.012

Ganzetti, M., Wenderoth, N., & Mantini, D. (2015). Mapping pathological changes in brain structure by combining T1- and T2-weighted MR imaging data. *Neuroradiology*, *57*(9), 917–928. https://doi.org/10.1007/s00234-015-1550-4

Garrity, A. G., Godfrey D. Pearlson, M. D., Kristen McKiernan, P. D., Dan Lloyd, P. D., Kent A. Kiehl, P. D., & Vince D. Calhoun, P. D. (2007). Aberrant "Default Mode" Functional Connectivity in Schizophrenia. *American Journal of Psychiatry*. https://doi.org/10.1176/ajp.2007.164.3.450

Geiger, M. J., Domschke, K., Ipser, J., Hattingh, C., Baldwin, D. S., Lochner, C., & Stein, D. J. (2016). Altered executive control network resting-state connectivity in social anxiety disorder. *The World Journal of Biological Psychiatry*, *17*(1), 47–57. https://doi.org/10.3109/15622975.2015.1083613

Geng, H., Wang, Y., Gu, R., Luo, Y.-J., Xu, P., Huang, Y., & Li, X. (2018). Altered brain activation and connectivity during anticipation of uncertain threat in trait anxiety. *Human Brain Mapping*, *39*(10), 3898–3914. https://doi.org/10.1002/hbm.24219

Gidron, Y. (2013). Trait Anxiety. In M. D. Gellman & J. R. Turner (Eds.), *Encyclopedia of Behavioral Medicine* (pp. 1989–1989). Springer. https://doi.org/10.1007/978-1-4419-1005-9_1539

Gollo, L. L., Mirasso, C., Sporns, O., & Breakspear, M. (2014). Mechanisms of Zero-Lag Synchronization in Cortical Motifs. *PLoS Computational Biology*, *10*(4), e1003548. https://doi.org/10.1371/journal.pcbi.1003548

Gramfort, A., Luessi, M., Larson, E., Engemann, D. A., Strohmeier, D., Brodbeck, C., Goj, R., Jas, M., Brooks, T., Parkkonen, L., & Hämäläinen, M. (2013). MEG and EEG data analysis with MNE-Python. *Frontiers in Neuroscience*, *7*, 267. https://doi.org/10.3389/fnins.2013.00267

Granger, C. W. J. (1969). Investigating Causal Relations by Econometric Models and Cross-spectral Methods. *Econometrica*, *37*(3), 424–438. https://doi.org/10.2307/1912791

Greicius, M. D., Supekar, K., Menon, V., & Dougherty, R. F. (2009). Resting-State Functional Connectivity Reflects Structural Connectivity in the Default Mode Network. *Cerebral Cortex*, *19*(1), 72–78. https://doi.org/10.1093/cercor/bhn059

Grupe, D. W., & Nitschke, J. B. (2013). Uncertainty and anticipation in anxiety: An integrated neurobiological and psychological perspective. *Nature Reviews Neuroscience*, *14*(7), 488–501. https://doi.org/10.1038/nrn3524

Gu, Y., Gu, S., Lei, Y., & Li, H. (2020). From Uncertainty to Anxiety: How Uncertainty Fuels Anxiety in a Process Mediated by Intolerance of Uncertainty. *Neural Plasticity*, *2020*(1), 8866386. https://doi.org/10.1155/2020/8866386

Hahn, A., Stein, P., Windischberger, C., Weissenbacher, A., Spindelegger, C., Moser, E., Kasper, S., & Lanzenberger, R. (2011). Reduced resting-state functional connectivity between amygdala and orbitofrontal cortex in social anxiety disorder. *NeuroImage*, *56*(3), 881–889. https://doi.org/10.1016/j.neuroimage.2011.02.064

Haufe, S., Nikulin, V. V., Müller, K.-R., & Nolte, G. (2013). A critical assessment of connectivity measures for EEG data: A simulation study. *NeuroImage*, *64*, 120–133. https://doi.org/10.1016/j.neuroimage.2012.09.036

Heilbronner, S. R., & Hayden, B. Y. (2016). Dorsal Anterior Cingulate Cortex: A Bottom-Up View. *Annual Review of Neuroscience*, *39*(Volume 39, 2016), 149–170. https://doi.org/10.1146/annurev-neuro-070815-013952

Hein, T. P., de Fockert, J., & Ruiz, M. H. (2021). State anxiety biases estimates of uncertainty and impairs reward learning in volatile environments. *NeuroImage*, *224*, 117424. https://doi.org/10.1016/j.neuroimage.2020.117424

Hein, T. P., Gong, Z., Ivanova, M., Fedele, T., Nikulin, V., & Herrojo Ruiz, M. (2023). Anterior cingulate and medial prefrontal cortex oscillations underlie learning alterations in trait anxiety in humans. *Communications Biology*, *6*(1), 1–17. https://doi.org/10.1038/s42003-023-04628-1

Hindriks, R., & Tewarie, P. K. B. (2023). Dissociation between phase and power correlation networks in the human brain is driven by co-occurrent bursts. *Communications Biology*, *6*(1), 1–13. https://doi.org/10.1038/s42003-023-04648-x

Hohenfeld, C., Werner, C. J., & Reetz, K. (2018). Resting-state connectivity in neurodegenerative disorders: Is there potential for an imaging biomarker? *NeuroImage: Clinical*, *18*, 849–870. https://doi.org/10.1016/j.nicl.2018.03.013

Honey, C. J., Sporns, O., Cammoun, L., Gigandet, X., Thiran, J. P., Meuli, R., & Hagmann, P. (2009). Predicting human resting-state functional connectivity from structural connectivity. *Proceedings of the National Academy of Sciences*, *106*(6), 2035–2040. https://doi.org/10.1073/pnas.0811168106

Iglesias, S., Mathys, C., Brodersen, K. H., Kasper, L., Piccirelli, M., den Ouden, H. E. M., & Stephan, K. E. (2013). Hierarchical prediction errors in midbrain

and basal forebrain during sensory learning. *Neuron*, *80*(2), 519–530. https://doi.org/10.1016/j.neuron.2013.09.009

Iglesias, S., Mathys, C., Brodersen, K. H., Kasper, L., Piccirelli, M., den Ouden, H. E. M., & Stephan, K. E. (2019). Hierarchical Prediction Errors in Midbrain and Basal Forebrain during Sensory Learning. *Neuron*, *101*(6), 1196–1201. https://doi.org/10.1016/j.neuron.2019.03.001

Imperatori, C., Farina, B., Adenzato, M., Valenti, E. M., Murgia, C., Marca, G. D., Brunetti, R., Fontana, E., & Ardito, R. B. (2019). Default mode network alterations in individuals with high-trait-anxiety: An EEG functional connectivity study. *Journal of Affective Disorders*, *246*, 611–618. https://doi.org/10.1016/j.jad.2018.12.071

Ioakeimidis, V., Lennuyeux-Comnene, L., Khachatoorian, N., Gaigg, S. B., Haenschel, C., Kyriakopoulos, M., & Dima, D. (2023). Trait and State Anxiety Effects on Mismatch Negativity and Sensory Gating Event-Related Potentials. *Brain Sciences*, *13*(10), 1421. https://doi.org/10.3390/brainsci13101421

Ivanova, M., Germanova, K., Petelin, D. S., Ragimova, A., Kopytin, G., Volel, B. A., Nikulin, V. V., & Herrojo Ruiz, M. (2025). Frequency-specific changes in prefrontal activity associated with maladaptive belief updating in volatile environments in euthymic bipolar disorder. *Translational Psychiatry*, *15*(1), 1–12. https://doi.org/10.1038/s41398-025-03225-6

Kelejian, H. H., & Prucha, I. R. (1999). A Generalized Moments Estimator for the Autoregressive Parameter in a Spatial Model. *International Economic Review*, *40*(2), 509–533. https://doi.org/10.1111/1468-2354.00027

Kim, S. M., Park, S. Y., Kim, Y. I., Son, Y. D., Chung, U.-S., Min, K. J., & Han, D. H. (2015). Affective network and default mode network in depressive adolescents with disruptive behaviors. *Neuropsychiatric Disease and Treatment*, *12*, 49–56. https://doi.org/10.2147/NDT.S95541

Knill, D. C., & Pouget, A. (2004). The Bayesian brain: The role of uncertainty in neural coding and computation. *Trends in Neurosciences*, *27*(12), 712–719. https://doi.org/10.1016/j.tins.2004.10.007

Knyazev, G. G., Savostyanov, A. N., & Levin, E. A. (2004). Alpha oscillations as a correlate of trait anxiety. *International Journal of Psychophysiology*, *53*(2), 147–160. https://doi.org/10.1016/j.ijpsycho.2004.03.001

Kobayashi, K., & Hsu, M. (2017). Neural Mechanisms of Updating under Reducible and Irreducible Uncertainty. *The Journal of Neuroscience*, *37*(29), 6972–6982. https://doi.org/10.1523/JNEUROSCI.0535-17.2017

Lachaux, J. P., Rodriguez, E., Martinerie, J., & Varela, F. J. (1999). Measuring phase synchrony in brain signals. *Human Brain Mapping*, *8*(4), 194–208. https://doi.org/10.1002/(sici)1097-0193(1999)8:4<194::aid-hbm4>3.0.co;2-c

Lang, E. W., Tomé, A. M., Keck, I. R., Górriz-Sáez, J. M., & Puntonet, C. G. (2012). Brain Connectivity Analysis: A Short Survey. *Computational Intelligence and Neuroscience*, *2012*, e412512. https://doi.org/10.1155/2012/412512

LeDoux, J. (2007). The amygdala. *Current Biology*, *17*(20), R868–R874. https://doi.org/10.1016/j.cub.2007.08.005

Li, N., Ma, N., Liu, Y., He, X.-S., Sun, D.-L., Fu, X.-M., Zhang, X., Han, S., & Zhang, D.-R. (2013). Resting-State Functional Connectivity Predicts Impulsivity in Economic Decision-Making. *Journal of Neuroscience*, *33*(11), 4886–4895. https://doi.org/10.1523/JNEUROSCI.1342-12.2013

Liddle, E. B., Hollis, C., Batty, M. J., Groom, M. J., Totman, J. J., Liotti, M., Scerif, G., & Liddle, P. F. (2011). Task-related default mode network modulation and inhibitory control in ADHD: Effects of motivation and methylphenidate. *Journal of Child Psychology and Psychiatry*, *52*(7), 761–771. https://doi.org/10.1111/j.1469-7610.2010.02333.x

Liu, C.-H., Guo, J., Lu, S.-L., Tang, L.-R., Fan, J., Wang, C.-Y., Wang, L., Liu, Q.-Q., & Liu, C.-Z. (2018). Increased Salience Network Activity in Patients With Insomnia Complaints in Major Depressive Disorder. *Frontiers in Psychiatry*, *9*. https://doi.org/10.3389/fpsyt.2018.00093

Lynch, C. J., Uddin, L. Q., Supekar, K., Khouzam, A., Phillips, J., & Menon, V. (2013). Default Mode Network in Childhood Autism: Posteromedial Cortex Heterogeneity and Relationship with Social Deficits. *Biological Psychiatry*, *74*(3), 212–219. https://doi.org/10.1016/j.biopsych.2012.12.013

Madhyastha, T. M., Askren, M. K., Boord, P., & Grabowski, T. J. (2015). Dynamic Connectivity at Rest Predicts Attention Task Performance. *Brain Connectivity*, *5*(1), 45–59. https://doi.org/10.1089/brain.2014.0248

Manoliu, A., Meng, C., Brandl, F., Doll, A., Tahmasian, M., Scherr, M., Schwerthöffer, D., Zimmer, C., Förstl, H., Bäuml, J., Riedl, V., Wohlschläger, A., & Sorg, C. (2014). Insular dysfunction within the salience network is associated

with severity of symptoms and aberrant inter-network connectivity in major depressive disorder. *Frontiers in Human Neuroscience*, *7*. https://doi.org/10.3389/fnhum.2013.00930

Mathews, A., & MacLeod, C. (2005). Cognitive Vulnerability to Emotional Disorders. *Annual Review of Clinical Psychology*, *1*(Volume 1, 2005), 167–195. https://doi.org/10.1146/annurev.clinpsy.1.102803.143916

Mathys, C. D., Daunizeau, J., Friston, K. J., & Stephan, K. E. (2011). A bayesian foundation for individual learning under uncertainty. *Frontiers in Human Neuroscience*, *5*, 39. https://doi.org/10.3389/fnhum.2011.00039

Mathys, C. D., Lomakina, E. I., Daunizeau, J., Iglesias, S., Brodersen, K. H., Friston, K. J., & Stephan, K. E. (2014). Uncertainty in perception and the Hierarchical Gaussian Filter. *Frontiers in Human Neuroscience*, *8*, 825. https://doi.org/10.3389/fnhum.2014.00825

Meijering, E. (2010). Neuron tracing in perspective. *Cytometry Part A*, *77A*(7), 693–704. https://doi.org/10.1002/cyto.a.20895

Menon, V. (2011). Large-scale brain networks and psychopathology: A unifying triple network model. *Trends in Cognitive Sciences*, *15*(10), 483–506. https://doi.org/10.1016/j.tics.2011.08.003

Nicholson, A. A., Harricharan, S., Densmore, M., Neufeld, R. W. J., Ros, T., McKinnon, M. C., Frewen, P. A., Théberge, J., Jetly, R., Pedlar, D., & Lanius, R. A. (2020). Classifying heterogeneous presentations of PTSD via the default mode, central executive, and salience networks with machine learning. *NeuroImage: Clinical*, *27*, 102262. https://doi.org/10.1016/j.nicl.2020.102262

Nolte, G., Bai, O., Wheaton, L., Mari, Z., Vorbach, S., & Hallett, M. (2004). Identifying true brain interaction from EEG data using the imaginary part of coherency. *Clinical Neurophysiology*, *115*(10), 2292–2307. https://doi.org/10.1016/j.clinph.2004.04.029

Nolte, G., Ziehe, A., Nikulin, V. V., Schlögl, A., Krämer, N., Brismar, T., & Müller, K.-R. (2008). Robustly estimating the flow direction of information in complex physical systems. *Physical Review Letters*, *100*(23), 234101. https://doi.org/10.1103/PhysRevLett.100.234101

Nunez, P. L., Srinivasan, R., Westdorp, A. F., Wijesinghe, R. S., Tucker, D. M., Silberstein, R. B., & Cadusch, P. J. (1997). EEG coherency. I: Statistics, reference electrode, volume conduction, Laplacians, cortical imaging, and interpreta-

tion at multiple scales. *Electroencephalography and Clinical Neurophysiology*, *103*(5), 499–515. https://doi.org/10.1016/s0013-4694(97)00066-7

Öngür, D., Lundy, M., Greenhouse, I., Shinn, A. K., Menon, V., Cohen, B. M., & Renshaw, P. F. (2010). Default mode network abnormalities in bipolar disorder and schizophrenia. *Psychiatry Research: Neuroimaging*, *183*(1), 59–68. https://doi.org/10.1016/j.pscychresns.2010.04.008

Ossadtchi, A., Altukhov, D., & Jerbi, K. (2018). Phase shift invariant imaging of coherent sources (PSIICOS) from MEG data. *NeuroImage*, *183*, 950–971. https://doi.org/10.1016/j.neuroimage.2018.08.031

Osten, P., & Margrie, T. W. (2013). Mapping brain circuitry with a light microscope. *Nature Methods*, *10*(6), 515–523. https://doi.org/10.1038/nmeth.2477

Padmanabhan, A., Lynch, C. J., Schaer, M., & Menon, V. (2017). The Default Mode Network in Autism. *Biological Psychiatry: Cognitive Neuroscience and Neuroimaging*, *2*(6), 476–486. https://doi.org/10.1016/j.bpsc.2017.04.004

Palaniyappan, L., Mallikarjun, P., Joseph, V., White, T. P., & Liddle, P. F. (2011). Reality distortion is related to the structure of the salience network in schizophrenia. *Psychological Medicine*, *41*(8), 1701–1708. https://doi.org/10.1017/S0033291710002205

Palaniyappan, L., & Liddle, P. F. (2012). Does the salience network play a cardinal role in psychosis? An emerging hypothesis of insular dysfunction. *Journal of Psychiatry and Neuroscience*, *37*(1), 17–27. https://doi.org/10.1503/jpn.100176

Parks, E. L., & Madden, D. J. (2013). Brain Connectivity and Visual Attention. *Brain Connectivity*, *3*(4), 317–338. https://doi.org/10.1089/brain.2012.0139

Paulus, M. P., Feinstein, J. S., Simmons, A., & Stein, M. B. (2004). Anterior cingulate activation in high trait anxious subjects is related to altered error processing during decision making. *Biological Psychiatry*, *55*(12), 1179–1187. https://doi.org/10.1016/j.biopsych.2004.02.023

Pellegrini, F., Delorme, A., Nikulin, V., & Haufe, S. (2023). Identifying good practices for detecting inter-regional linear functional connectivity from EEG. *NeuroImage*, *277*, 120218. https://doi.org/10.1016/j.neuroimage.2023.120218

Peng, Z. W., Xu, T., He, Q. H., Shi, C. Z., Wei, Z., Miao, G. D., Jing, J., Lim, K. O., Zuo, X. N., & Chan, R. C. K. (2014). Default network connectivity

as a vulnerability marker for obsessive compulsive disorder. *Psychological Medicine*, *44*(7), 1475–1484. https://doi.org/10.1017/S0033291713002250

Pierce, D. A. (1971). Least squares estimation in the regression model with autoregressive-moving average errors. *Biometrika*, *58*(2), 299–312. https://doi.org/10.1093/biomet/58.2.299

Piray, P., & Daw, N. D. (2021). A model for learning based on the joint estimation of stochasticity and volatility. *Nature Communications*, *12*(1), 6587. https://doi.org/10.1038/s41467-021-26731-9

Powers, A. R., Mathys, C., & Corlett, P. R. (2017). Pavlovian conditioning-induced hallucinations result from overweighting of perceptual priors. *Science (New York, N.Y.)*, *357*(6351), 596–600. https://doi.org/10.1126/science.aan3458

Prater, K. E., Hosanagar, A., Klumpp, H., Angstadt, M., & Luan Phan, K. (2013). Aberrant Amygdala–Frontal Cortex Connectivity During Perception of Fearful Faces and at Rest in Generalized Social Anxiety Disorder. *Depression and Anxiety*, *30*(3), 234–241. https://doi.org/10.1002/da.22014

Pulcu, E., & Browning, M. (2019). The Misestimation of Uncertainty in Affective Disorders. *Trends in Cognitive Sciences*, *23*(10), 865–875. https://doi.org/10.1016/j.tics.2019.07.007

Raichle, M. E. (2015). The Brain's Default Mode Network. *Annual Review of Neuroscience*, *38*(Volume 38, 2015), 433–447. https://doi.org/10.1146/annurev-neuro-071013-014030

Rao, R. P. N., & Ballard, D. H. (1999). Predictive coding in the visual cortex: A functional interpretation of some extra-classical receptive-field effects. *Nature Neuroscience*, *2*(1), 79–87. https://doi.org/10.1038/4580

Reess, T. J., Rus, O. G., Schmidt, R., de Reus, M. A., Zaudig, M., Wagner, G., Zimmer, C., van den Heuvel, M. P., & Koch, K. (2016). Connectomics-based structural network alterations in obsessive-compulsive disorder. *Translational Psychiatry*, *6*(9), e882–e882. https://doi.org/10.1038/tp.2016.163

Rolls, E., Treves, A., Rolls, E., & Treves, A. (1997). *Neural Networks and Brain Function*. Oxford University Press.

Rolls, E. T., Deco, G., Huang, C.-C., & Feng, J. (2022). The human orbitofrontal cortex, vmPFC, and anterior cingulate cortex effective connectome: Emotion, memory, and action. *Cerebral Cortex (New York, N.Y.: 1991)*, *33*(2), 330–356. https://doi.org/10.1093/cercor/bhac070

Saviola, F., Pappaianni, E., Monti, A., Grecucci, A., Jovicich, J., & De Pisapia, N. (2020). Trait and state anxiety are mapped differently in the human brain. *Scientific Reports*, *10*(1), 11112. https://doi.org/10.1038/s41598-020-68008-z

Schoffelen, J. M., & Gross, J. (2019). Studying dynamic neural interactions with MEG. *541*. https://doi.org/10.1007/978-3-030-00087-5_18
Accepted: 2020-05-04T20:30:34Z

Schulreich, S., & Schwabe, L. (2021). Causal Role of the Dorsolateral Prefrontal Cortex in Belief Updating under Uncertainty. *Cerebral Cortex (New York, N.Y.: 1991)*, *31*(1), 184–200. https://doi.org/10.1093/cercor/bhaa219

Seeley, W. W., Menon, V., Schatzberg, A. F., Keller, J., Glover, G. H., Kenna, H., Reiss, A. L., & Greicius, M. D. (2007). Dissociable intrinsic connectivity networks for salience processing and executive control. *The Journal of Neuroscience: The Official Journal of the Society for Neuroscience*, *27*(9), 2349–2356. https://doi.org/10.1523/JNEUROSCI.5587-06.2007

Seguin, C., Sporns, O., & Zalesky, A. (2023). Brain network communication: Concepts, models and applications. *Nature Reviews Neuroscience*, *24*(9), 557–574. https://doi.org/10.1038/s41583-023-00718-5

Sehlmeyer, C., Dannlowski, U., Schöning, S., Kugel, H., Pyka, M., Pfleiderer, B., Zwitserlood, P., Schiffbauer, H., Heindel, W., Arolt, V., & Konrad, C. (2011). Neural correlates of trait anxiety in fear extinction. *Psychological Medicine*, *41*(4), 789–798. https://doi.org/10.1017/S0033291710001248

Shadli, S. M., Ando, L. C., McIntosh, J., Lodhia, V., Russell, B. R., Kirk, I. J., Glue, P., & McNaughton, N. (2021). Right frontal anxiolytic-sensitive EEG 'theta' rhythm in the stop-signal task is a theory-based anxiety disorder biomarker. *Scientific Reports*, *11*(1), 19746. https://doi.org/10.1038/s41598-021-99374-x

Singer, W. (1999). Neuronal synchrony: A versatile code for the definition of relations? *Neuron*, *24*(1), 49–65, 111–125. https://doi.org/10.1016/s0896-6273(00)80821-1

Smallwood, J., Bernhardt, B. C., Leech, R., Bzdok, D., Jefferies, E., & Margulies, D. S. (2021). The default mode network in cognition: A topographical perspective. *Nature Reviews Neuroscience*, *22*(8), 503–513. https://doi.org/10.1038/s41583-021-00474-4

Spielberger, C. D. (1983). Manual for the State-Trait Anxiety Inventory. *APA PsycTests*.

Sporns, O. (2013). Structure and function of complex brain networks. *Dialogues in Clinical Neuroscience*, *15*(3), 247. https://doi.org/10.31887/DCNS.2013.15.3/osporns

Stefanics, G., Heinzle, J., Horváth, A. A., & Stephan, K. E. (2018). Visual Mismatch and Predictive Coding: A Computational Single-Trial ERP Study. *The Journal of Neuroscience*, *38*(16), 4020–4030. https://doi.org/10.1523/JNEUROSCI.3365-17.2018

Sylvester, C. M., Corbetta, M., Raichle, M. E., Rodebaugh, T. L., Schlaggar, B. L., Sheline, Y. I., Zorumski, C. F., & Lenze, E. J. (2012). Functional network dysfunction in anxiety and anxiety disorders. *Trends in Neurosciences*, *35*(9), 527–535. https://doi.org/10.1016/j.tins.2012.04.012

Székely, A., Balog, P., Benkö, E., Breuer, T., Székely, J., Kertai, M. D., Horkay, F., Kopp, M. S., & Thayer, J. F. (2007). Anxiety Predicts Mortality and Morbidity After Coronary Artery and Valve Surgery—A 4-Year Follow-Up Study. *Psychosomatic Medicine*, *69*(7), 625–631. https://doi.org/10.1097/PSY.0b013e31814b8c0f

Szeszko, P. R., & Yehuda, R. (2019). Magnetic resonance imaging predictors of psychotherapy treatment response in post-traumatic stress disorder: A role for the salience network. *Psychiatry Research*, *277*, 52–57. https://doi.org/10.1016/j.psychres.2019.02.005

Taulu, S., & Hari, R. (2009). Removal of magnetoencephalographic artifacts with temporal signal-space separation: Demonstration with single-trial auditory-evoked responses. *Human Brain Mapping*, *30*(5), 1524–1534. https://doi.org/10.1002/hbm.20627

Thut, G., Miniussi, C., & Gross, J. (2012). The Functional Importance of Rhythmic Activity in the Brain. *Current Biology*, *22*(16), R658–R663. https://doi.org/10.1016/j.cub.2012.06.061

Uddin, L. Q., Kelly, A. M. C., Biswal, B. B., Margulies, D. S., Shehzad, Z., Shaw, D., Ghaffari, M., Rotrosen, J., Adler, L. A., Castellanos, F. X., & Milham, M. P. (2008). Network homogeneity reveals decreased integrity of default-mode network in ADHD. *Journal of Neuroscience Methods*, *169*(1), 249–254. https://doi.org/10.1016/j.jneumeth.2007.11.031

Uddin, L. Q., Yeo, B. T., & Spreng, R. N. (2019). Towards a universal taxonomy of macro-scale functional human brain networks. *Brain topography*, *32*(6), 926–942. https://doi.org/10.1007/s10548-019-00744-6

Ueda, H. R., Dodt, H.-U., Osten, P., Economo, M. N., Chandrashekar, J., & Keller, P. J. (2020). Whole-Brain Profiling of Cells and Circuits in Mammals by Tissue Clearing and Light-Sheet Microscopy. *Neuron*, *106*(3), 369–387. https://doi.org/10.1016/j.neuron.2020.03.004

Van Veen, B. D., van Drongelen, W., Yuchtman, M., & Suzuki, A. (1997). Localization of brain electrical activity via linearly constrained minimum variance spatial filtering. *IEEE transactions on bio-medical engineering*, *44*(9), 867–880. https://doi.org/10.1109/10.623056

Vidaurre, C., Nolte, G., de Vries, I. E. J., Gómez, M., Boonstra, T. W., Müller, K.-R., Villringer, A., & Nikulin, V. V. (2019). Canonical maximization of coherence: A novel tool for investigation of neuronal interactions between two datasets. *NeuroImage*, *201*, 116009. https://doi.org/10.1016/j.neuroimage.2019.116009

Viriyopase, A., Bojak, I., Zeitler, M., & Gielen, S. (2012). When Long-Range Zero-Lag Synchronization is Feasible in Cortical Networks. *Frontiers in Computational Neuroscience*, *6*. https://doi.org/10.3389/fncom.2012.00049

Wang, M., Cao, L., Li, H., Xiao, H., Ma, Y., Liu, S., Zhu, H., Yuan, M., Qiu, C., & Huang, X. (2021). Dysfunction of Resting-State Functional Connectivity of Amygdala Subregions in Drug-Naïve Patients With Generalized Anxiety Disorder. *Frontiers in Psychiatry*, *12*, 758978. https://doi.org/10.3389/fpsyt.2021.758978

Wang, W., Junhong, Li, & and Ding, R. (2011). Maximum likelihood parameter estimation algorithm for controlled autoregressive autoregressive models. *International Journal of Computer Mathematics*, *88*(16), 3458–3467. https://doi.org/10.1080/00207160.2011.598514

Ward, L. M. (2003). Synchronous neural oscillations and cognitive processes. *Trends in Cognitive Sciences*, *7*(12), 553–559. https://doi.org/10.1016/j.tics.2003.10.012

Winkler, I., Panknin, D., Bartz, D., Müller, K.-R., & Haufe, S. (2016). Validity of time reversal for testing Granger causality. *IEEE Transactions on Signal Processing*, *64*(11), 2746–2760. https://doi.org/10.1109/TSP.2016.2531628

Wittayer, M., Weber, C. E., Krämer, J., Platten, M., Schirmer, L., Gass, A., & Eisele, P. (2023). Exploring (peri-) lesional and structural connectivity tissue damage through T1/T2-weighted ratio in iron rim multiple sclerosis lesions. *Magnetic Resonance Imaging*, *95*, 12–18. https://doi.org/10.1016/j.mri.2022.10.009

Xu, J., Van Dam, N. T., Feng, C., Luo, Y., Ai, H., Gu, R., & Xu, P. (2019). Anxious brain networks: A coordinate-based activation likelihood estimation meta-analysis of resting-state functional connectivity studies in anxiety. *Neuroscience & Biobehavioral Reviews*, *96*, 21–30. https://doi.org/10.1016/j.neubiorev.2018.11.005

Yeh, C.-H., Jones, D. K., Liang, X., Descoteaux, M., & Connelly, A. (2021). Mapping Structural Connectivity Using Diffusion MRI : Challenges and Opportunities. *Journal of Magnetic Resonance Imaging*, *53*(6), 1666–1682. https://doi.org/10.1002/jmri.27188

Zhao, X.-H., Wang, P.-J., Li, C.-B., Hu, Z.-H., Xi, Q., Wu, W.-Y., & Tang, X.-W. (2007). Altered default mode network activity in patient with anxiety disorders: An fMRI study. *European Journal of Radiology*, *63*(3), 373–378. https://doi.org/10.1016/j.ejrad.2007.02.006

Zhou, W., Feng, Z., Xu, Y. F., Wang, X., & Lv, H. (2020). Empirical Fourier Decomposition: An Accurate Adaptive Signal Decomposition Method.

Zhu, L., Liu, Y., Liu, R., Peng, Y., Cao, J., Li, J., & Kong, W. (2023). Decoding Multi-Brain Motor Imagery From EEG Using Coupling Feature Extraction and Few-Shot Learning. *IEEE transactions on neural systems and rehabilitation engineering: a publication of the IEEE Engineering in Medicine and Biology Society*, *31*, 4683–4692. https://doi.org/10.1109/TNSRE.2023.3336356

Zhu, X., Wang, X., Xiao, J., Liao, J., Zhong, M., Wang, W., & Yao, S. (2012). Evidence of a Dissociation Pattern in Resting-State Default Mode Network Connectivity in First-Episode, Treatment-Naive Major Depression Patients. *Biological Psychiatry*, *71*(7), 611–617. https://doi.org/10.1016/j.biopsych.2011.10.035

Appendix A. Total number of epochs

Table A1: Number of total epochs chosen for the analysis per subject after preprocessing

Subject	N Epochs	Subject	N Epochs
S1	320	S21	320
S2	303	S22	319
S3	320	S23	312
S4	313	S24	276
S5	264	S25	191
S6	318	S26	320
S7ˆ	155	S27	134
S8	320	S28	309
S9	320	S29	320
S10	311	S30	179
S11	301	S31	320
S12	315	S32	320
S13	255	S33	313
S14	318	S34	320
S15	318	S35	216
S16ˆ	159	S36	320
S17	304	S37	320
S18	0	S38	239
S19	320	S39	320

Notes. ˆ indicates participants with only one experimental block

Appendix B. Uncorrected p-value matrices

This appendix provides the uncorrected p-value matrices for three frequency bands in two time intervals: *a).* early (0-0.5) and *b).* late (0.5-1).

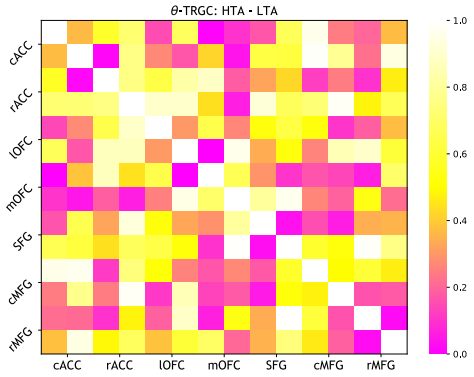

(a) Early post-outcome interval

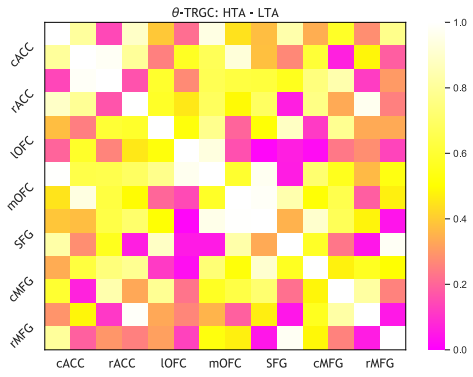

(b) Late post-outcome interval

Figure B1: Uncorrected p-value matrices for θ-band connections.

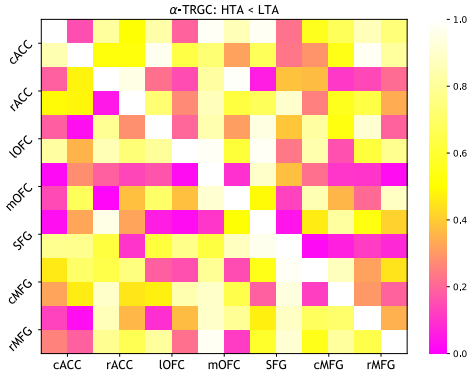

(a) Early post-outcome interval

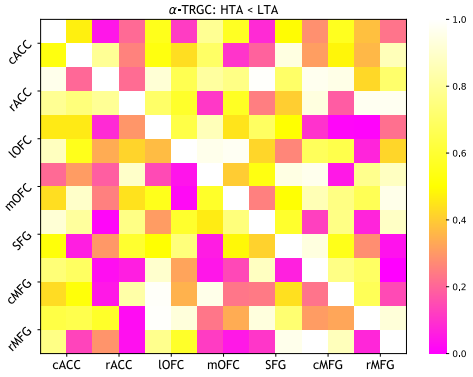

(b) Late post-outcome interval

Figure B2: Uncorrected p-value matrices for α-band connections.

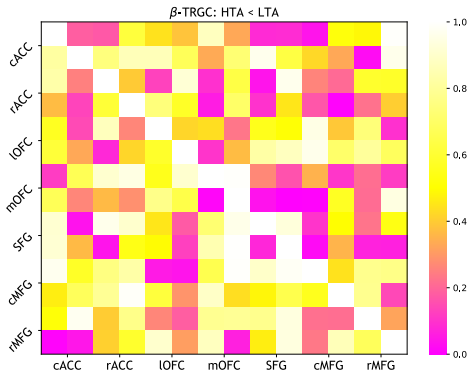

(a) Early post-outcome interval

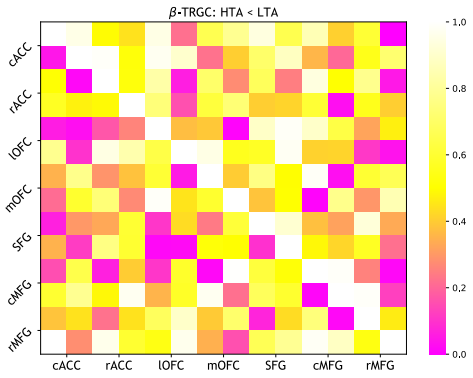

(b) Late post-outcome interval

Figure B3: Uncorrected p-value matrices for β-band connections.